Chapter 3

Modulation of Coordination Environment: A Convenient Approach to Tailor Magnetic Anisotropy in Seven Coordinate Co(II) Complexes

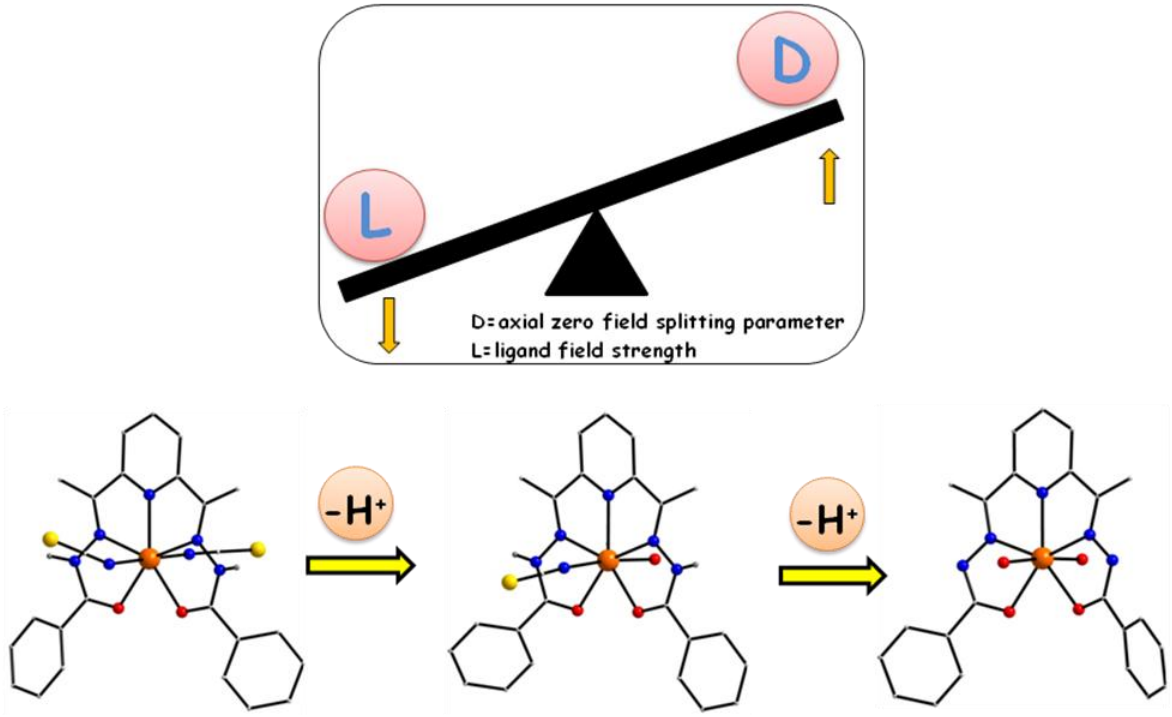

Abstract: The possibility to control magnetic anisotropy by tuning contribution of second order perturbation to spin-orbit coupling through modulation of coordination environment has been investigated. Magnetic anisotropy of a series of mononuclear seven coordinate Co(II) complexes have been systematically investigated by using low temperature magnetization measurements and density functional theory based calculations. Subtle variation of the coordination environment triggers remarkable deviation in the axial zero field splitting parameter of mononuclear seven coordinate Co(II) complexes.

3.1. Introduction

Large uniaxial magnetic anisotropy is widely recognized as an essential criterion for enhancement of blocking temperature of magnetization reversal in single molecular magnets (SMM) [1-5]. Even single ion species with strong uniaxial anisotropy are reported to behave as SMM with large energy barrier for magnetization reversal [6-14]. In view of this, efforts to rationally manipulate the magnetic anisotropy of molecular species have intensified during the last few years [15-16]. However, parameters governing magnetic anisotropy are poorly understood and intricate control over magnetic anisotropy has remained one of the most formidable challenges.

It is well established that magnetic anisotropy is primarily induced by spin-orbit coupling which is operative as a first order perturbation or a second order perturbation. In transition metal complexes, orbital degeneracy is lifted by crystal field splitting and Jahn-Teller effect. Thus, orbital angular momentum is quenched and this in turn minimizes spin-orbit interaction. Recent studies have established that in low coordinate 3d complexes with a symmetric and weak ligand environment, quenching of orbital angular momentum is significantly reduced as the d-orbitals lie within a narrow energy gap. Increasing magnetic anisotropy by adopting unconventional coordination geometry has emerged as a promising strategy for enhancing energy barrier for magnetization reversal in SMMs [17-20]. For example, due to large uniaxial anisotropy in mononuclear two coordinate Fe(I) complex, record energy barrier for magnetisation reversal has been observed [20]. However, low coordinate species are stable only under inert atmosphere and this severely limits their possible utility in different applications. In this context, an approach to induce magnetic anisotropy in high coordinate transition metal species is highly desirable.

Contribution to spin-orbit coupling through second order perturbation may occur through spin-orbit interaction of an orbitally non-degenerate ground state with a low lying orbitally degenerate excited state. Thus, even in species with orbitally non-degenerate electronic ground state, there is a possibility to both induce and control magnetic anisotropy by appropriate manipulation of excited state energy levels. This approach allows designing magnetically anisotropic building blocks with higher coordination number. In this regard, seven coordinate pentagonal bipyramidal (PBP) 3d complexes are found to be particularly appealing as a few examples with large uniaxial anisotropy have been already reported [21-29, 49].

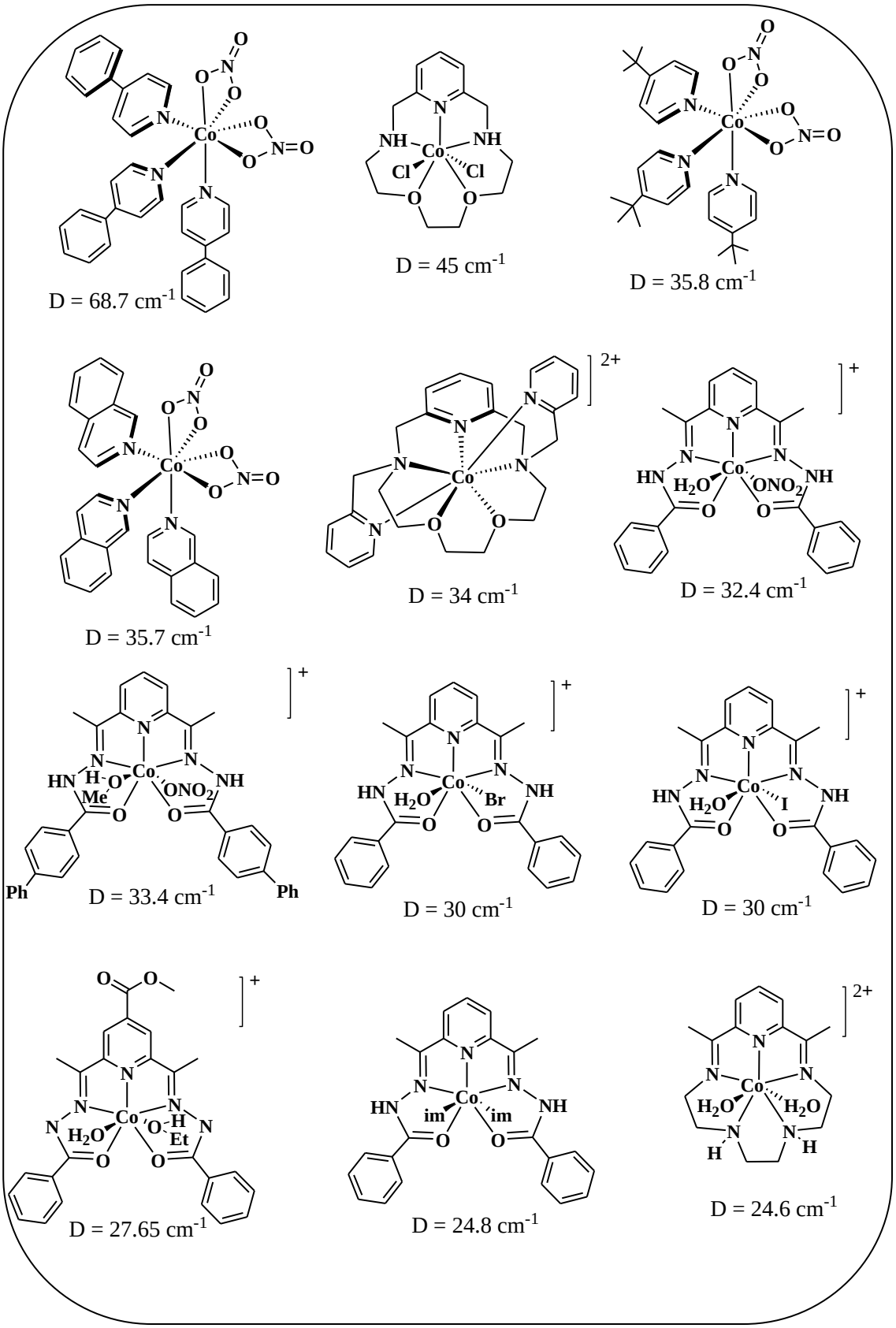

Chart 3.1. Examples of seven coordinate Co(II) complexes for which D values have been determined

The planer pentadentate acyclic ligand 2,6-diacetylpyridine bis(benzoyl hydrazone) (H_2L) is known to stabilize many transition metal ions in heptacoordinate PBP geometry [27]. PBP Fe(II) and Ni(II) complexes formed by H_2L ligand have strong uniaxial anisotropy and associated with characteristic large negative axial zero field splitting parameters (D) [21-25, 30]. However, the zero field splitting parameter of Co(II) complexes of the ligand H_2L was found to be large positive and all of them show slow relaxation of magnetization under a small applied field (Chart 3.1) [25-33, 48]. The origin of this large positive D parameter lies in spin-orbit coupling stemming from mixing of the ground electronic level with two excited electronic levels. Thus, in principle it should be possible to control magnetic anisotropy by tuning the mixing of ground electronic state with the excited electronic states. Therefore, it is anticipated that appropriate modulation of the coordination environment can act as a versatile approach to control magnetic anisotropy. However, without comprehensive understanding of the electronic states involved in spin-orbit mixing, it is not viable to undertake such investigations. Therefore, systematic studies on coordination environment mediated control of magnetic anisotropy are very rare [34].

In this chapter, the synthesis, characterization and magnetic properties of six mononuclear Co(II) complexes *viz*. $[Co(H_2L)(H_2O)_2](NO_3)_2.2H_2O$ (**5**), $[Co(H_2L)(SCN)_2].3H_2O$ (**6**), $[Co(H_2L)(SCN)_2].4H_2O$ (**7**), $[Co(HL)(SCN)(H_2O)]$ (**8**), $[Co(HL)(H_2O)_2](NO_3).H_2O$ (**9**) and $[Co(L)(H_2O)_2]$ (**10**) have been elaborated. The D value for all the compounds were determined using magnetization measurements and the experimental results have been rationalized with the help of theoretical calculations. Moreover, superoxide dismutase activity of these compounds has been studied spectrophotometrically using indirect Nitro Blue Tetrazolium (NBT) assay.

3.2. Experimental Section

3.2.1. Materials and Methods

Starting materials were procured from commercial sources and used as received. Solvents were purified by conventional techniques and distilled prior to use. 2,6-diacetylpyridine bis(benzoyl hydrazone), $[Co(H_2L)(H_2O)(NO_3)]NO_3$ and $[Ni(N_3)_2(dpa)_2].H_2O$ (dpa: 2,2'-dipyridyl amine) were prepared following a published procedure [35-36]. Elemental analyses were performed on a Perkin Elmer Model PR 2400 Series II Elemental Analyzer. Infrared spectra were recorded on a Nicolet Impact

I-410 FT-IR spectrometer as KBr diluted discs and a Perkin Elmer MIR-FIR FT-IR spectrometer. A Shimadzu UV-visible 2550 Spectrophotometer was used to record the UV-visible spectra. Melting points were recorded on a Buchi M-560 Melting Point apparatus and are reported uncorrected. Magnetic susceptibility data were collected on microcrystalline samples over a 2-300 K temperature range with an applied field of 1000 Oe using a MPMS SQUID magnetometer. Magnetization studies were performed between 0-5 T at 2 K, 5 K, 7 K and 10 K.

3.2.2. Synthesis of $[Co(H_2L)(H_2O)_2](NO_3)_2.2H_2O$ (5)

To a solution of $[Co(H_2L)(H_2O)(NO_3)]NO_3$) (0.03 mmol, 0.0196 g) in 10 mL methanol, $Na_3[FeF_6]$ (0.03 mmol, 0.0072 g) dissolved in 10 mL distilled water was added. The reaction mixture stirred at room temperature for an hour and then filtered. The filtrate was kept undisturbed for slow evaporation at room temperature. Orange plate shaped crystals were observed after 14 days. The mother liquor was discarded and crystals were washed with ethanol followed by diethyl ether and then air dried. Yield: 0.015 g (78 % based on Co); M. p. >250°C; Elemental analysis: Found C, 41.73%; H, 4.30%; N, 15.17%. $C_{23}H_{29}N_7O_{12}Co$ requires C, 42.22%; H, 4.47%; N, 14.98%. IR (KBr, cm^{-1}): 3424(br), 1629(m), 1522(m), 1490(m), 1430(w), 1374(m), 1162(m), 1053(w), 809(w), 705(m), 528(w).

3.2.3. Synthesis of $[Co(H_2L)(SCN)_2].3H_2O$ (6)

To a solution of $[Co(H_2L)(H_2O)(NO_3)]NO_3$ (0.015 mmol, 0.010 g) in 10 mL methanol, a solution of KSCN (0.05 mmol, 0.005 g) dissolved in 10 mL H_2O was added. The reaction mixture was stirred at room temperature for an hour during which the colour of the solution turned from bright orange to yellow. The reaction mixture was filtered and the filtrate was kept undisturbed for slow evaporation at room temperature. Brown needle shaped crystals were observed after a week. The mother liquor was decanted and crystals were washed with minimum amount of ethanol and then dried with diethyl ether. Yield: 0.007 g (76 % based on Co); M. p. >250°C; Elemental analysis: Found C, 47.91%; H, 4.31%; N, 16.12%. $C_{25}H_{27}N_7O_5S_2Co$ requires C, 47.79%; H, 4.33%; N, 15.60%. IR (KBr, cm^{-1}): 3558(br), 2074(s), 1620(s), 1520(m), 1444(m), 1380(w), 1283(s), 1178(s), 1078(m), 801(m), 714(m), 466(w).

3.2.4. Synthesis of $[Co(H_2L)(SCN)_2].4H_2O$ (7)

To a solution of $[Co(H_2L)(H_2O)(NO_3)]NO_3$ (0.027 mmol, 0.017 g) in 15 mL methanol, KSCN (0.027 mmol, 0.003 g) dissolved in 10 mL distilled water was added and the whole was stirred at room temperature for 3 hours. The reaction mixture was filtered and the filtrate was kept undisturbed for slow evaporation at room temperature. Red block shaped crystals were observed after 2 months. The mother liquor was discarded and crystals were washed with ethanol followed by diethyl ether and then air dried. Yield: 0.014 g (83 % based on Co); M. p. >250°C; Elemental analysis: Found C, 45.94%; H, 4.66%; N, 14.92%. $C_{25}H_{29}N_7O_6S_2Co$ requires C, 46.46%; H, 4.52%; N, 15.16%. IR (KBr, cm^{-1}): 3016(br), 2108(m), 2086(m), 1628(m), 1493(m), 1367(m), 1310(m), 1163(m), 1053(w), 903(w), 715(m), 420(w).

3.2.5. Synthesis of $[Co(HL)(H_2O)(SCN)]$ (8)

To a solution of $[Co(H_2L)(H_2O)(NO_3)]NO_3$ (0.027 mmol, 0.017 g) in 20 mL methanol, KSCN (0.027 mmol, 0.003 g) dissolved in 10 mL distilled water was added and the whole was stirred at room temperature for 3 hours. Then, $Na_2[Fe(CN)_5(NO)].2H_2O$ (0.027 mmol, 0.008 g) dissolved in 5 mL distilled was added and again stirred for an hour. The reaction mixture was filtered and the filtrate was kept undisturbed for slow evaporation at room temperature. Pink block shaped crystals were observed after 1 month. The mother liquor was discarded and crystals were washed with ethanol followed by diethyl ether and then air dried. Yield: 0.010 g (72 % based on Co); M. p. >250°C; Elemental analysis: Found C, 53.01%; H, 4.07%; N, 15.11%. $C_{24}H_{23}N_6O_3SCo$ requires C, 53.95%; H, 4.34%; N, 15.72%. IR (KBr, cm^{-1}): 3198(br), 2088(m), 1628(m), 1493(m), 1422(w), 1367(m), 1285(m), 1160(m), 1043(w), 897(w), 800(w), 710(m), 596(w), 437(w).

3.2.6. Synthesis of $[Co(HL)(H_2O)_2](NO_3).H_2O$ (9)

To a solution of $[Co(H_2L)(H_2O)(NO_3)]NO_3$ (0.03 mmol, 0.0196 g) in 10 mL methanol, $K_3[Fe(CN)_6]$ (0.005 mmol, 0.0017 g) dissolved in 10 mL distilled water was added without agitation. The reaction mixture was kept in dark undisturbed for slow evaporation at room temperature. Orange block shaped crystals were observed after 20 days. The mother liquor was discarded and crystals were washed with ethanol followed by diethyl ether and then air dried. Yield: 0.008 g (57 % based on Co); M. p. >250°C;

Elemental analysis: Found C, 60.77%; H, 5.09%; N, 15.52%. $C_{23}H_{27}N_5O_2Co$ requires C, 60.51%; H, 5.71%; N, 14.70%. IR (KBr, cm^{-1}): 3400(br), 1629(m), 1577(m), 1520(m), 1487(w), 1373(m), 1261(m), 1023(w), 867(w), 801(w), 713(m), 689(m).

3.2.7. Synthesis of $[Co(L)(H_2O)_2]$ (10)

To a solution of $[Co(H_2L)(NO_3)(H_2O)]NO_3$ (0.015 mmol, 0.010 g) in 20 mL ethanol, $[Ni(N_3)_2(dpa)_2].H_2O$ (0.027 mmol, 0.013 g) was added and the whole was heated in a water bath for an hour. The reaction mixture was cooled, filtered and the filtrate was kept undisturbed for slow evaporation at room temperature. Bright orange needle shaped crystals were observed after 24 hours. The mother liquor was discarded and crystals were washed with ethanol followed by diethyl ether and then air dried. Yield: 0.007 g (81 % based on Co); M. p. >250°C; Elemental analysis: Found C, 56.13%; H, 4.71%; N, 14.55%. $C_{23}H_{23}N_5O_4Co$ requires C, 56.11%; H, 4.71%; N, 14.22%. IR (KBr, cm^{-1}): 3251(br), 1677(w), 1579(m), 1498(s), 1411(w), 1371(s), 1163(m), 1046(m), 992(w), 903(w), 796(m), 690(m), 422(w).

3.2.8. Determination of SOD activity

The SOD activity of the Co(II) complexes were measured by using a modified nitro blue tetrazolium (NBT) assay [37-38]. Reduction of NBT by alkaline DMSO, which acts as a source of superoxide radical ion ($O_2^{-\cdot}$) produces a blue formazan dye which can be easily detected spectrophotometrically. The % inhibition of NBT reduction was monitored against different concentration of the mononuclear Co(II) complexes. In general, 100 µL of 1.5 mM NBT was added to 1.5 mL of 0.2 M potassium phosphate buffer (pH 7.8). The tubes were kept in ice for 15 minutes. Then, 1.4 mL of alkaline DMSO solution was added with stirring. The absorbance was recorded at 630 nm against a sample prepared under similar condition except the addition of NaOH in DMSO. The compounds were added to the above condition before the addition of alkaline DMSO. Each experiment was performed in duplicate for different concentrations of the compounds. The concentration required to produce 50% inhibition (IC_{50}) of the reduction of NBT has been determined by linear fitting of the curve.

3.2.9. Single Crystal X-Ray Diffraction Studies

Single crystals of all the compounds suitable for diffraction measurements were used directly from the reaction mixtures. The diffraction data for the compounds were collected on a Bruker APEX-II CCD diffractometer using MoKα radiation (λ=0.71073 Å) using φ and ω scans of narrow (0.5°) frames at 90-100 K. All the structures were solved by direct methods using SHELXL-97 as implemented in the WinGX program system [39]. Anisotropic refinement was executed on all non-hydrogen atoms. The aliphatic and aromatic hydrogen atoms were placed on calculated positions but were allowed to ride on their parent atoms during subsequent cycles of refinements. Positions of N-H and O-H hydrogen atoms were located on a difference Fourier map and allowed to ride on their parent atoms during subsequent cycles of refinements. Crystallographic data (excluding structure factors) have been deposited with the Cambridge Crystallographic Data Centre, CCDC, 12 Union Road, Cambridge CB21EZ, UK. Copies of the data can be obtained free of charge on quoting the depository number CCDC 1421271 (**6**) and CCDC 1421272 (**10**). The crystal data and refinement parameters of all the compounds are listed in Table 3.2.

Continuous SHAPE analysis of the coordination environment around the central Co(II) atom of all the compounds was performed [40]. The results obtained from shape analysis of all the mononuclear Co(II) compounds are listed in Table 3.1.

Table 3.1. Shape analysis data for compounds **5**-**10** using SHAPE program

Complex	HP-7	HPY-7	PBPY-7	COC-7	CTPR-7	JPBPY-7	JETPY-7
5	33.278	23.871	0.254	6.919	5.080	3.179	23.327
6	33.690	24.451	0.250	7.328	5.594	2.928	23.584
7	31.943	22.961	0.522	6.773	4.827	3.283	20.906
8	33.199	23.181	0.507	6.866	4.944	3.263	21.807
9	33.920	23.936	0.190	7.328	5.641	3.412	23.563
10	33.442	23.167	0.341	6.568	5.210	3.134	23.771

HP-7: Heptagon (D_{7h}); HPY-7: Hexagonal pyramid (C_{6v}); PBPY-7: Pentagonal bipyramid (D_{5h}); COC-7: Capped octahedron (C_{3v}); CTPR-7: Capped trigonal prism (C_{2v}); JPBPY-7: Johnson pentagonal bipyramid J13 (D_{5h}); JETPY-7: Johnson elongated triangular pyramid J7 (C_{3v})

Table 3.2. Crystal data and refinement parameters of compounds **5**-**10**

Complex	**5**	**6**	**7**	**8**	**9**	**10**
Empirical formula	$C_{23}H_{27}N_7O_{12}Co$	$C_{25}H_{21}N_7O_5S_2Co$	$C_{25}H_{21}N_7O_6S_2Co$	$C_{24}H_{23}N_6O_3SCo$	$C_{23}H_{24}N_6O_8Co$	$C_{23}H_{21}N_5O_4Co$
Formula weight	652.44	622.54	646.60	534.47	571.41	490.38
Temperature/K	296	100	296	296	296	100
Crystal system	Orthorhombic	Orthorhombic	Monoclinic	Triclinic	Triclinic	Orthorhombic
Space group	*Pbca*	$P2_12_12_1$	$P2_1/n$	*P-1*	*P-1*	$Cmc2_1$
a/Å	16.098 (6)	10.692 (2)	11.340 (2)	9.004 (3)	9.836 (6)	26.039 (11)
b/Å	14.623 (5)	11.464 (2)	15.881 (2)	11.889 (4)	9.939 (6)	11.404 (5)
c/Å	24.781 (8)	24.031 (5)	16.022 (2)	11.996 (4)	14.886 (8)	7.328 (4)
α/°	90.00	90.00	90.00	74.79 (2)	91.72 (4)	90.00
β/°	90.00	90.00	98.13 (1)	79.48 (2)	107.79 (4)	90.00
γ/°	90.00	90.00	90.00	78.83 (2)	106.63 (4)	90.00
Volume/$Å^3$	5833.9 (4)	2945.6 (10)	2856.5 (7)	1204.06 (7)	1316.63 (14)	2176.35 (18)
Z	8	4	4	2	2	4
ρ_{calc}, g cm^{-3}	1.486	1.404	1.503	1.471	1.441	1.497
μ/mm^{-1}	0.661	0.771	0.800	0.838	0.739	0.830
Crystal size, mm^3	0.16x0.14x0.12	0.25x0.17x0.11	0.32x0.21x0.14	0.46x0.37x0.11	0.24x0.16x0.12	0.32x0.08x0.06
F(000)	2696	1276	1340	522	590	1012
Data/parameters/restraints	5714/420/2	5758/370/2	8470/412/0	5616/326/0	6327/363/5	1815/162/1
Goodness-of-fit on F^2	1.032	1.100	1.058	0.998	0.929	1.209
Final R indexes [I>=2σ (I)]	R_1=0.0462; wR_2=0.1082	R_1= 0.0370; wR_2=0.0938	R_1= 0.0344 ; wR_2=0.0864	R_1= 0.0370; wR_2=0.0956	R_1= 0.0749; wR_2=0.1850	R_1= 0.0340; wR_2=0.0900
Final R indexes [all data]	R_1= 0.0876 ; wR_2=0.1269	R_1= 0.0443; wR_2=0.1070	R_1= 0.0463 ; wR_2=0.0963	R_1= 0.0614; wR_2=0.1184	R_1= 0.1537 ; wR_2=0.2177	R_1= 0.0432 ; wR_2=0.1232

3.2.10. Theoretical Calculations

DFT level single point calculations were carried on the experimental structures using the ORCA program package [41]. For the transition metal centre, i.e. Co(II) ion Stuttgart/Dresden ECPs (SDD) basis sets and the def2-TZVP Ahlrichs basis set for Coulomb fitting, i.e. def2-TZVP/J is used [42]. For all other atoms def2 basis set of the Ahlrich group along with TZVP basis set was used [43]. A hybrid DFT functional, B3LYP was used for all DFT calculations [44]. Since all the complexes are open shell systems with spin multiplicity greater than 1, unrestricted Kohn-Sham (UKS) wavefunction was used. To be on the safe side of SCF convergence of DFT calculation, NoFinalGrid keyword and spin-orbit operator based on mean-field approach are applied. For calculating contribution of spin-orbit coupling to the D tensor, Coupled-Perturbed (CP) method is used as it uses revised pre-factors for the spin-flip terms. Meanwhile for evaluating spin-spin contribution to D tensor, Breit-Pauli type operator is used along with canonical orbitals for the spin-density of the system.

3.3. Results and Discussions

3.3.1. Synthesis and characterization of $[Co(H_2L)(H_2O)_2](NO_3)_2.2H_2O$ (5)

When $[Co(H_2L)(H_2O)(NO_3)]NO_3$ was allowed to react with pre-synthesized $Na_3[FeF_6]$ in a methanol-water medium, it was anticipated that the $[FeF_6]^{3-}$ will bind with the precursor Co(II) complex through a fluoride bridge and thus result in the formation of a heteronuclear species. Contrary to our anticipation, the reaction resulted in the formation of compound **5** as orange plate shaped crystals in good yield (Scheme 3.1). Single crystals of compound **5** are stable at room temperature. Compound **5** was further characterized by elemental analysis, FT-IR and single crystal X-ray diffraction study.

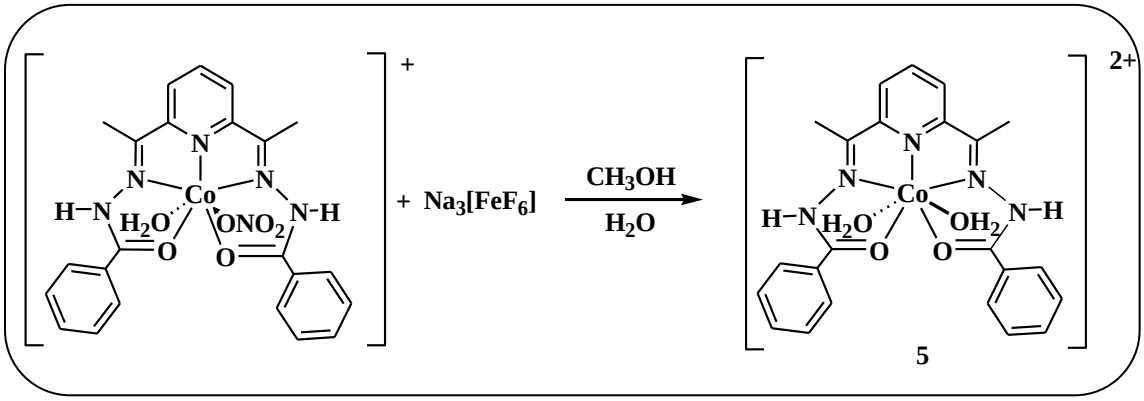

Scheme 3.1. Synthesis of compound **5**

Results obtained from the elemental analysis are in good agreement with the proposed formulation of compound **5**. The FT-IR spectrum of compound **5** recorded as KBr disc is depicted in Figure 3.1. A broad band due to the -OH stretching of the coordinated water molecules is observed at 3434 cm^{-1}. Strong absorption band observed at 1629 cm^{-1} can be attributed to the C=N stretching vibration of the imine group from the bis-hydrazone ligand. The absorption peak at 1374 cm^{-1} in the spectrum is due the C=C stretching vibration of phenyl rings present in the ligand H_2L.

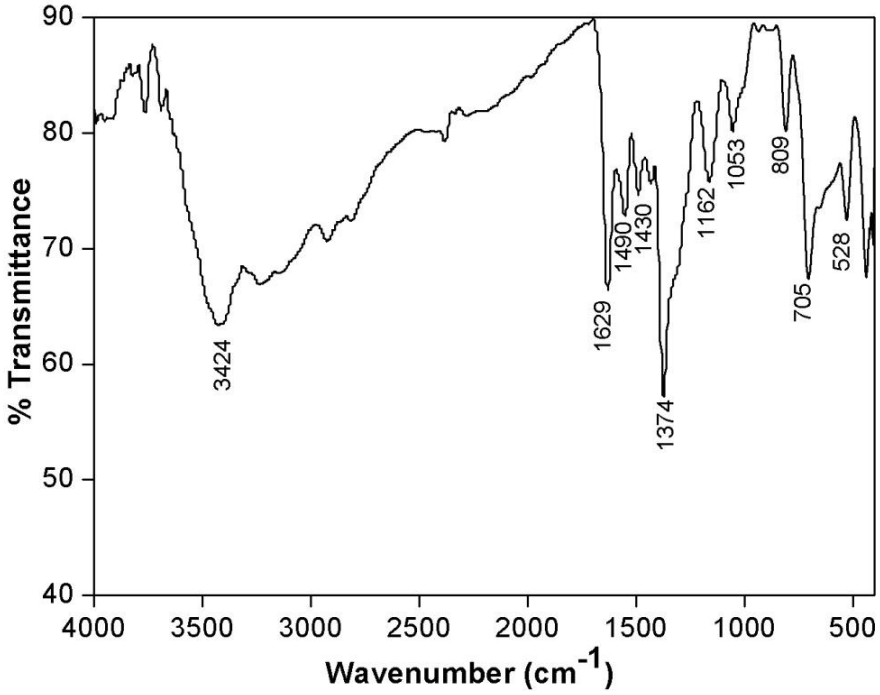

Figure 3.1. FT-IR spectrum of compound **5** as KBr diluted discs

3.3.2. Synthesis and characterization of $[Co(H_2L)(SCN)_2].3H_2O$ (6) and $[Co(H_2L)(SCN)_2].4H_2O$ (7)

Two novel mononuclear seven coordinate PBP Co(II) complexes, $[Co(H_2L)(SCN)_2].3H_2O$ (**6**) and $[Co(H_2L)(SCN)_2].4H_2O$ (**7**) were prepared starting from the parent compound $[Co(H_2L)(H_2O)(NO_3)]NO_3$. When the reaction of $[Co(H_2L)(H_2O)(NO_3)]NO_3$ dissolved in methanol was carried out in presence of two equivalents of aqueous KSCN solution, it resulted in the formation of the formation of brown needle shaped crystals of compound **6** in good yield (Scheme 3.2). As anticipated, the two axial sites of the precursor complex was replaced by two nitrogen atoms thiocyanate ligands leading to the formation of compound **6** with three lattice water molecules.

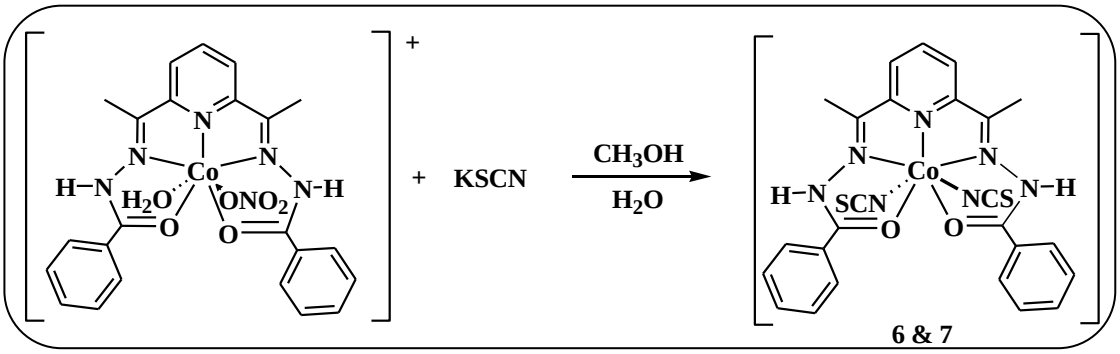

Scheme 3.2. Synthesis of compounds **6** and **7**

Further, when the reaction was repeated by using equimolar amounts of the precursor Co(II) complex and KSCN in same reaction medium, it resulted in the formation of compound **7** as red block shaped crystals. Single crystals of compound **7** possess four water molecules in the crystal lattice. This eventually gives rise to a different supramolecular organization within the crystal lattice. Both the compounds retain their crystallinity in room temperature. Single crystals of compounds **6** and **7** were characterized with the aid of elemental analysis, FT-IR and single crystal X-ray diffraction studies.

Elemental analysis data obtained for both compounds **6** and **7** are in good agreement with that obtained from the proposed formulation of the compounds. The FT-IR spectra of compounds **6** and **7** are depicted in Figure 3.2 and Figure 3.3 respectively. Both the spectra feature broad absorption band at 3558 and 3016 cm^{-1} respectively indicating the

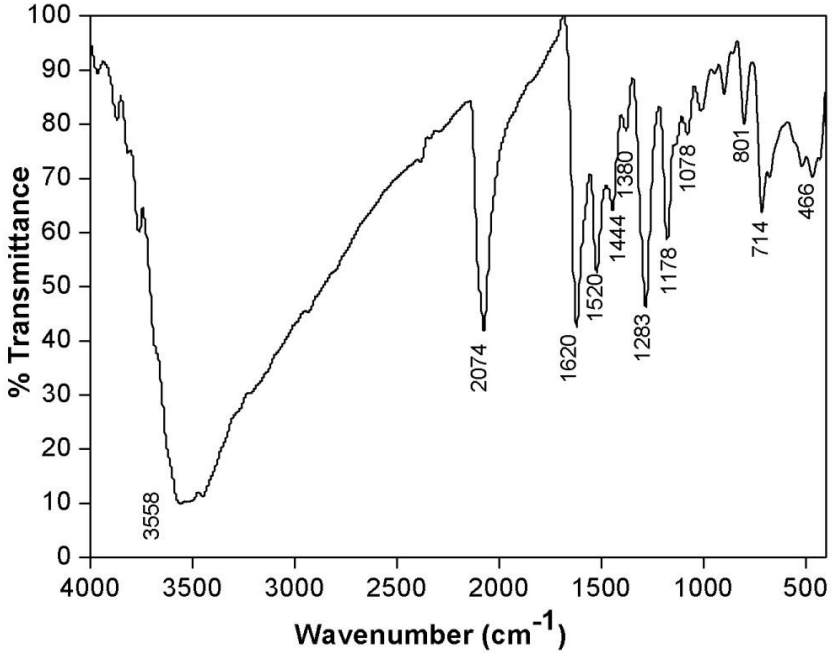

Figure 3.2. FT-IR spectrum of compound **6** as KBr diluted discs

presence of lattice water molecules. Strong absorption bands are observed at 2074 and 2086 cm^{-1} respectively which can be accounted for the C≡N stretching vibration of the axial thiocyanate ligands. The absorption peak due to the C=N stretching vibration of the imine group from the bis-hydrazone ligand are observed at 1620 and 1628 cm^{-1} respectively. Strong absorption peak observed at 1520 and 1493 cm^{-1} respectively can be assigned as the stretching frequency due to the phenyl ring of the ligand H_2L and the absorption peak due the N-C=O stretching vibration present in the ligand H_2L are observed at 1380 and 1367 cm^{-1} for compounds **6** and **7** in the spectra.

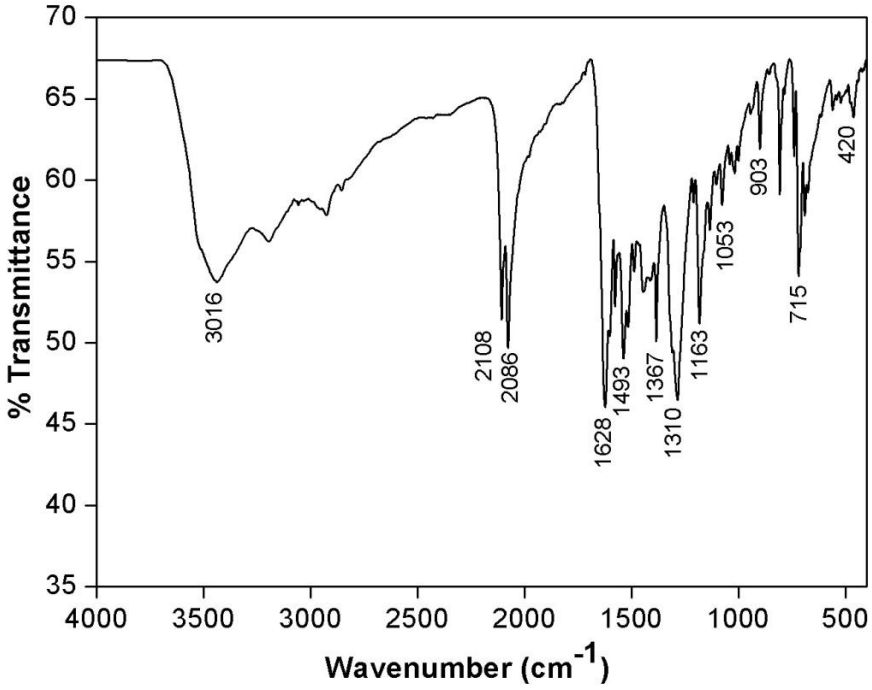

Figure 3.3. FT-IR spectrum of compound **7** as KBr diluted discs

3.3.3. Synthesis and characterization of [Co(HL)(SCN)(H_2O)] (8)

It has been established that [Mn(H_2L)(H_2O)Cl]Cl undergoes facile reaction with nitroprosside ion in presence of KSCN and form cyanobridged heterometallic aggregates [45]. When the Co(II) analogue of the same ligand, H_2L was allowed to react with nitroprusside in presence of KSCN, formation of heterometallic complex was not observed as anticipated (Scheme 3.3). Instead, a monoanionic species of the precursor complex was formed with one of the axial sites of the mononuclear precursor complex being substituted by thiocyanate ligand. Compound **8** is pink blocked shaped crystal isolated in good yield. Single crystals of compound **8** are further characterized with the help of elemental analysis, FT-IR and single crystal X-ray diffraction studies.

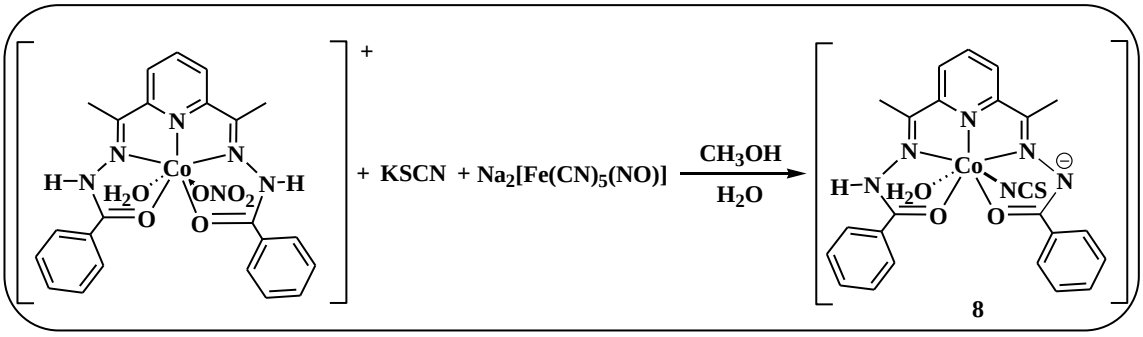

Scheme 3.3. Synthesis of compound **8**

Elemental analysis data obtained for compounds **8** agrees well with that calculated for the proposed formulation of the compound. The FT-IR spectrum of compound **8** is shown in Figure 3.4. The stretching due to the -OH bond of the coordinated water molecule is observed as a broad band at 3434 cm^{-1}. The sharp absorption band at 2088 cm^{-1} can be attributed to the C≡N stretching vibration of the axial thiocyanate ligand. The absorption band observed at 1628 cm^{-1} is due to the C=N stretching vibration of the imine group from the ligand HL. The absorption peak due the N-C=O stretching vibration present in the ligand HL was observed at 1367 cm^{-1} in the spectrum.

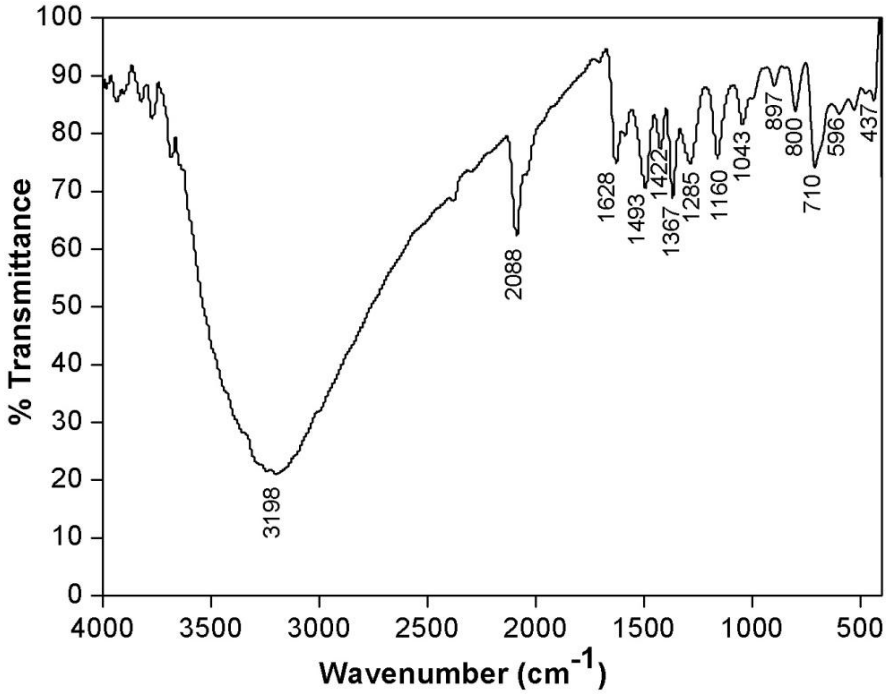

Figure 3.4. FT-IR spectrum of compound **8** as KBr diluted discs

3.3.4. Synthesis and characterization of $[Co(HL)(H_2O)_2](NO_3)H_2O$ (9)

Another monoanionic compound has been synthesized when the reaction of $[Co(H_2L)(H_2O)(NO_3)]NO_3$ was performed with aqueous $K_3[Fe(CN)_6]$ solution in one

sixth ratio. This reaction did not yield the expected heterometallic complex, but orange block shaped crystals of compound **9** was formed in good yield upon slow evaporation of the solvent at room temperature (Scheme 3.4). Aqueous solution of $K_3[Fe(CN)_6]$ is added in very dilute concentration and so it acted as a base in the abstraction of the N-H protons of the hydrazide moiety. Thus, a monoanionic species with both the axial sites of the PBP Co(II) center occupied by O atoms two water molecules is obtained. A nitrate ion is present in the lattice and thereby maintains the charge neutrality of the compound. Stable single crystals of compound **9** are characterized by elemental analysis, FT-IR and single crystal X-ray diffraction studies.

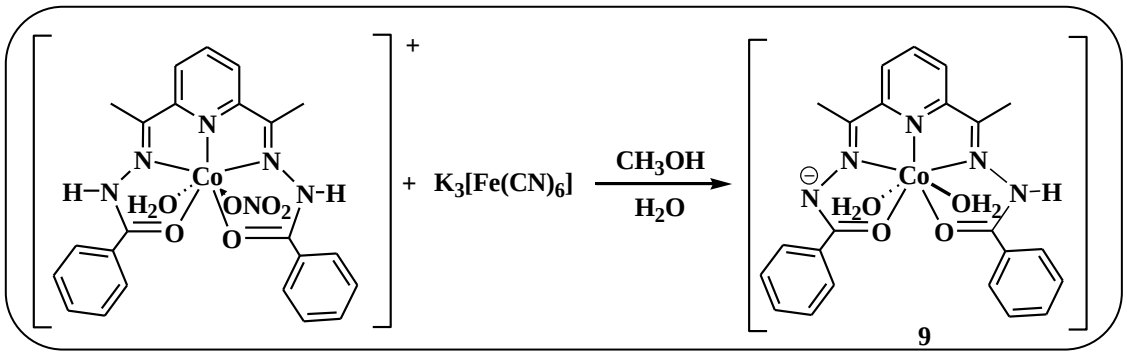

Scheme 3.4. Synthesis of compound **9**

A good agreement of the elemental analysis data has been obtained for compound **9** with that of the proposed formulation of the compound. The FT-IR spectrum of compound **9** as KBr diluted discs is depicted in Figure 3.5. Absorption peak at 3400

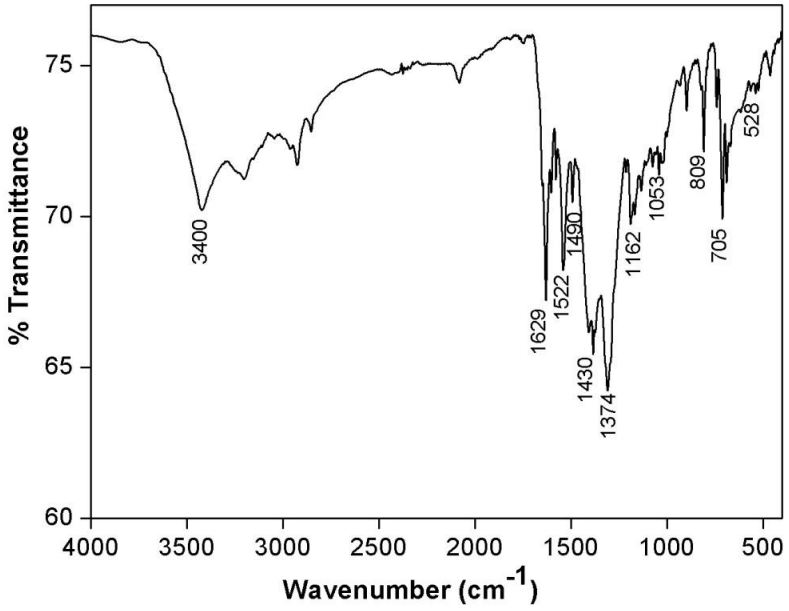

Figure 3.5. FT-IR spectrum of compound **9** as KBr diluted discs

cm^{-1} can be accounted for the presence of the water molecules present in the compound. The sharp absorption band observed at 1629 cm^{-1} is due to the stretching vibration of the ring of the bis-hydrazone ligand HL. The absorption peak due to the N-C=O stretching vibration of phenyl rings present in the ligand HL is observed at 1374 cm^{-1} in the spectrum.

3.3.5. Synthesis and characterization of $[Co(L)(H_2O)_2]$ (10)

We also attempted to bridge the PBP Co(II) precursor by an azido based metalloligand $[Ni(N_3)_2(dpa)_2].H_2O$ Thus, the ethanolic solution of the precursor complex, $[Co(H_2L)(H_2O)(NO_3)]NO_3$ was allowed to react with $[Ni(N_3)_2(dpa)_2(N_3)_2].H_2O$ with constant heating on a water bath (Scheme 3.5). Slow evaporation of the solvent at room temperature yielded orange needle shaped crystals of compound **10**.However, contrary to our anticipation, azido bridged heterometallic species was not isolated and compound **10** is a msononuclear PBP Co(II) complex containing a dianionic form of the bis-hydrazone ligand. Air stable single crystals of compound **10** are subjected to characterization by using elemental analysis, FT-IR and single crystal X-ray diffraction studies.

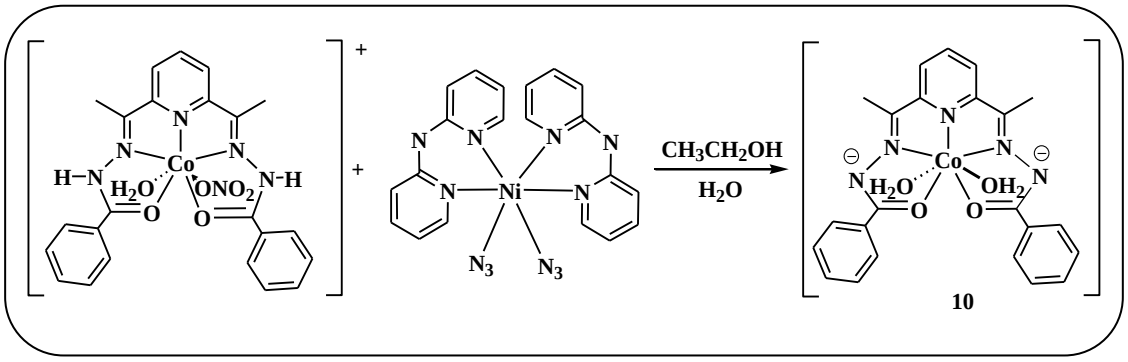

Scheme 3.5. Synthesis of compound **10**

Elemental analysis data obtained for compound **10** are in good agreement with that of the calculated value obtained from the proposed formulation of the compound. Figure 3.6 depicts the FT-IR spectrum of compound **10** as KBr diluted discs. A broad peak at 3251 cm^{-1} can be attributed to the presence of the coordinated water molecules present in the compound. The absorption band at 1677 cm^{-1} indicates the presence of C=N stretching vibration of the imine group from the bis-hydrazone ligand L. The sharp

absorption peak at 1374 and 1498 cm^{-1} in the spectrum can be attributed to the C=C stretching vibration of phenyl rings present in the ligand L.

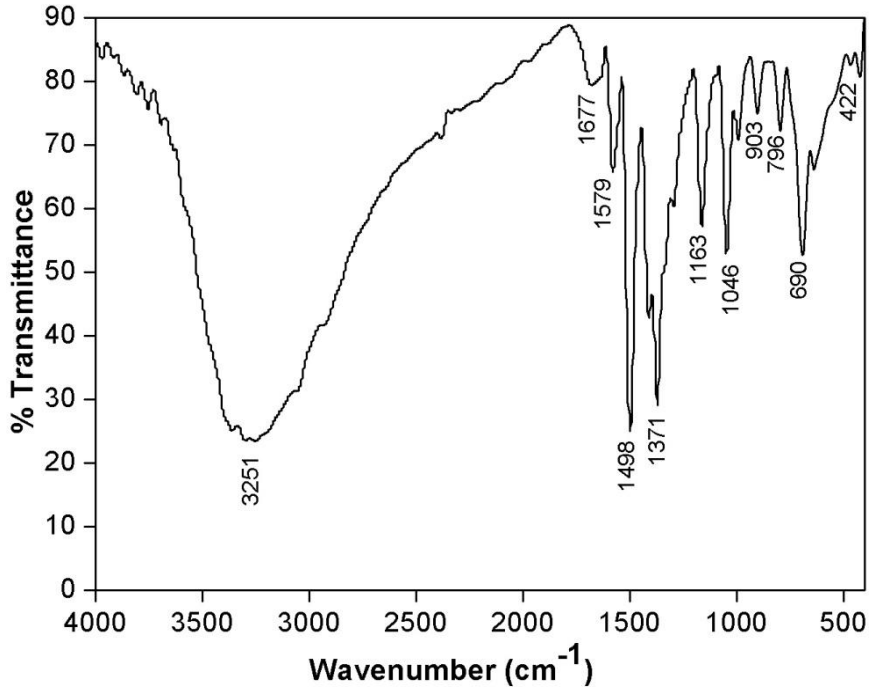

Figure 3.6. FT-IR spectrum of compound **10** as KBr diluted discs

3.3.6. Molecular structures of compounds 5-10

The molecular structures of compounds **5-10** were determined by single crystal X-ray diffraction technique. Representative view of the molecular structures of compounds **5-10** are depicted in Figure 3.7. Relevant crystal data along with the refinement parameters are given in Table 3.2. In all the six complexes, the PBP geometry of the precursor complex, $[Co(H_2L)(H_2O)(NO_3)]NO_3$ has been retained. The equatorial sites of all the compounds **5-10** have been occupied by the planar pentadentate bis-hydrazone ligand, H_2L. The Co(II) centre of these compounds are ligated to the pyridine nitrogen atom, two imine nitrogen atoms and two oxygen atoms of the hydrazide moiety in the equatorial environment. Continuous shape analysis using SHAPE software reveals that the geometry around Co(II) center in compounds **5-10** are D_{5h} PBP as the mean deviation from D_{5h} geometry is the least. Table 3.1 depicts the shape analyses data for compounds **5-10**. The five donor atoms from the pentadentate ligand form an ideal planar structure as the sum of the chelate angles and the bite angle O(1)-Co(1)-O(2) measures between 359.98° and 360.60° in all the compounds, which

confirms a planar equatorial environment for all the compounds. Important bond lengths and bond angles of compounds **5-10** are listed in Table 3.3.

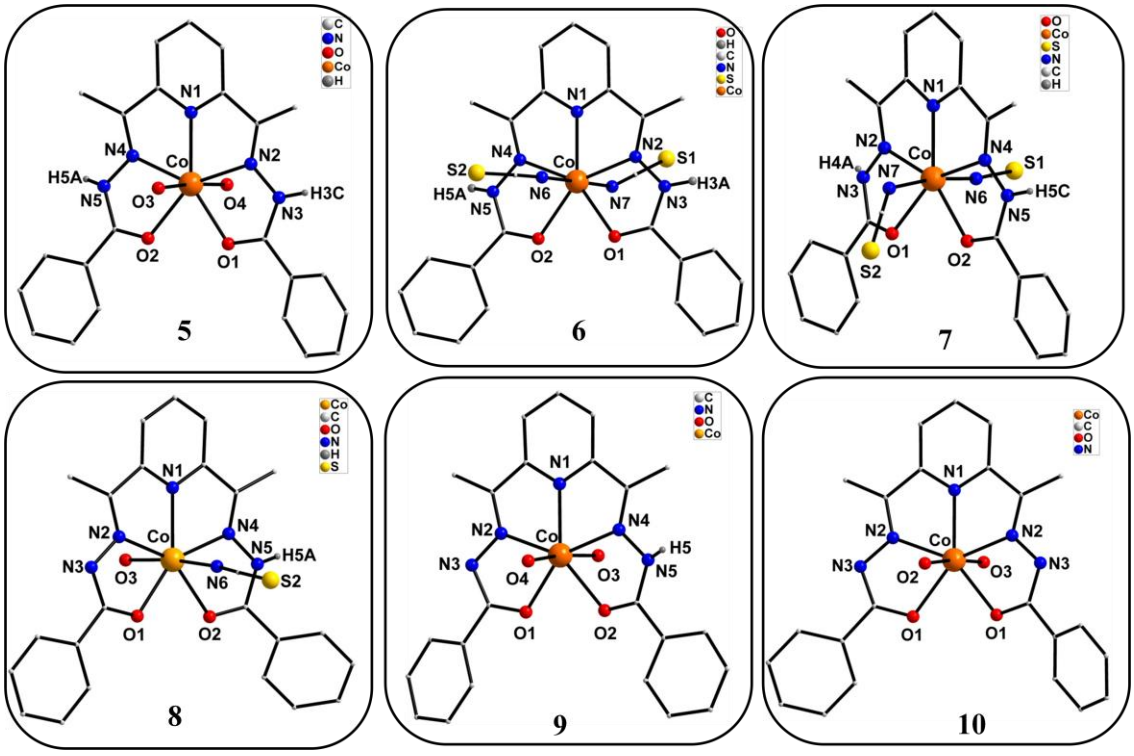

Figure 3.7. Molecular structures of compounds **5-10**. Aromatic and aliphatic hydrogen atoms are omitted for clarity. Only the N-H protons are shown wherever present

In compounds **5**, **6** and **7**, the pentadentate bis-hydrazone ligand, H_2L is in neutral >C=N=NH-C=O form with both the amido protons being retained. The electroneutrality of compound **5** is maintained by the presence of two nitrate groups in the crystal lattice. In compounds **6** and **7**, the axial sites of the central Co(II) atom are attached to two thiocyanate groups, thereby imparting electroneutrality to the compounds. The bis-hydrazone ligand is monoanionic in compounds **8** and **9** as an amido N-H proton is absent and thus leading to the formation of a >C=N=N$^-$-C=O linkage. One of the axial sites of the PBP central Co(II) atom of compound **8** is attached to a thiocyanate group and this eventually imparts electroneutrality to the compound. In case of compound **9**, the electroneutrality is maintained by the nitrate group present in the lattice. Moreover, a dianionic form of the pentadentate bis-hydrazone ligand, H_2L prevails in compound **10** with the removal of both the amido N-H protons. Both the axial sites of the Co(II) center are substituted by neutral H_2O molecules and thus the overall charge neutrality has been maintained without any ionic species in the crystal lattice. The equatorial Co-O bond distances for compounds **5**, **6**, **7**

and **10** are significantly longer than that of the reported precursor complex (2.150 and 2.229 Å). But in the compounds **8** and **9**, the equatorial Co-O bond distances are shorter than the precursor complex. However, one of the equatorial Co-O bond distances in compounds **8** (2.239 Å) and **9** (2.236 Å) are significantly longer than the other Co-O bond distance. The negative charge on the oxygen atom of the deprotonated α-oxiazine arm of the ligand strengthens the Co-O bonds and this eventually lengthens one of the Co-O bonds. Further, in case of compound **10**, where both the amido N-H protons are deprotonated, both the equatorial Co-O bond distances are longer than the precursor complex and are equal in length (2.260 Å). Both the amido N-H protons of the bis-hydrazone ligand are retained intact in compound **5**, **6** and **7**. In compounds **6** and **7**, both the axial sites of the PBP central Co(II) atom are occupied by two thiocyanate groups, thereby lending a N_5O_2 equatorial coordination environment. The axial

Table 3.3. Selected bond lengths (Å) and bond angles (◦) of compounds **5**-**10**

Bonds lengths	**5**	**6**	**7**	**8**	**9**	**10**
Co-N(1)	2.167(1)	2.187(3)	2.169(0)	2.191 (0)	2.163(1)	2.178(1)
Co-N(2)	2.190(1)	2.190(3)	2.191 (0)	2.148 (1)	2.158(1)	2.187(1)
Co-N(4)	2.194(1)	2.220(4)	2.203 (0)	2.270 (1)	2.220(1)	2.187(1)
Co-O(1)	2.190(1)	2.227(4)	2.242 (0)	2.138 (1)	2.138(1)	2.260(1)
Co-O(2)	2.195(1)	2.302(4)	2.209 (0)	2.379 (1)	2.236(1)	2.260(1)
Co-axial(1)	2.104(1)	2.078(4)	2.089 (0)	2.157 (1)	2.168(1)	2.119(1)
Co-axial(2)	2.095(1)	2.120(4)	2.107 (0)	2.073 (1)	2.114(1)	2.096(1)
Bond Angles	**5**	**6**	**7**	**8**	**9**	**10**
O(1)-Co(1)-N(2)	71.07(1)	70.02(8)	70.54(1)	72.21(2)	71.41(3)	69.57(1)
N(2)-Co(1)-N(1)	70.69(1)	70.83(8)	70.39(1)	71.51(2)	71.63(3)	70.80(1)
N(1)-Co(1)-N(4)	70.70(1)	70.33(8)	70.72(1)	69.02(2)	70.10(3)	70.80(1)
N(4)-Co(1)-O(2)	70.77(1)	71.62(8)	71.02(1)	67.60(2)	68.91(3)	69.57(1)
O(2)-Co(1)-O(1)	76.96(1)	77.41(8)	77.93(1)	79.64(2)	77.93(3)	79.57(1)
N(1)-Co(1)-axial(1)	88.04(1)	91.28(8)	95.15(1)	89.37(2)	90.30(3)	95.71(1)
N(1)-Co(1)-axial(2)	95.55(1)	89.20(8)	92.25(1)	96.34(2)	94.57(4)	89.10(1)

Axial(1): H_2O (**5**); SCN (**6** & **7**); H_2O (**8** & **9**); H_2O (**10**)

Axial(2): H_2O (**5**); SCN (**6** & **7**); SCN (**8**); H_2O (**9**); H_2O (**10**)

Co-N(thiocyanato) bond distances are 2.078 Å and 2.120 Å (**6**) and 2.089 Å and 2.107 Å (**7**) respectively. These Co-N(thiocyanato) bond distances are in good agreement with the Co-N bond distances observed for identical mononuclear PBP Co(II) complexes [56]. The coordination environment of compounds **5**, **9** and **10** are similar with both the axial sites of the mononuclear PBP Co(II) being occupied by water molecules. The axial Co-O(H_2O) bond distances are comparable with that of the reported Co-O(H_2O) bond distances of the precursor Co(II) complex. In compound **8**, one of the axial sites of the PBP central Co(II) atom is occupied by a H_2O molecule

Table 3.4. Hydrogen bonding parameters of compounds **5-10**

Complex	**Interactions**	**H···A (Å)**	**D···A(Å)**	**∠D–H···A(°)**	**Symmetry**
5	O(3)-H(3A)...O(1)	1.99	2.899(1)	171.0	1-x, -y, -z
	O(4)-H(4A)...O(9)	1.92	2.753(1)	170.0	x, ½-y, -½+z
	O(4)-H(4B)...O(100)	2.04	2.741(1)	176.0	x, ½-y, -½+z
	O(100)-H(101)...O(101)	1.85	2.752(1)	165.0	½ +x, y, ½ -z
	O(100)-H(102)...O(5)	2.18	2.965(1)	157.0	½ +x, y, ½ -z
7	N(3)-H(4A)...O(6)	2.02	2.778(1)	166.0	1+x, y, z
	O(4)-H(4B)...O(1)	2.05	2.829(1)	170.0	-1+x, y, z
	O(5)-H(5A)...S(1)	2.44	3.297(1)	171.0	1+x, -y, 1-z
	N(5)-H(5C)...O(7)	2.11	2.929(1)	166.0	1+x, y, z
	O(6)-H(6A)...S(2)	2.52	3.316(1)	163.0	-1+x, y, z
	O(6)-H(6B)...O(5)	1.99	2.788(1)	159.0	1-x, -y, 1-z
	O(7)-H(7A)...S(1)	2.51	3.329(1)	175.0	1-x, -y, 1-z
8	O(3)-H(3A)...O(1)	1.89	2.608(1)	168.0	1-x, 1-y, 1-z
	O(3)-H(3A)...O(2)	2.29	2.894(1)	136.0	1-x, 1-y, 1-z
9	O(3)-H(3A)...O(1)	2.20	2.769(2)	122.0	1-x, -y, 1-z
	O(3)-H(3B)...O(2)	1.97	2.767(2)	150.0	1-x, -y, 1-z
	O(4)-H(4A)...N(3)	1.99	2.846(2)	161.0	2-x, -y, 1-z
	O(4)-H(4B)...O(103)	2.08	2.965(2)	176.0	2-x, 1-y, 1-z
	N(5)-H(5)...O(100)	2.09	2.843(2)	161.0	1-x, 1-y, 1-z
10	O(4)-H(4A)...O(1)	1.99	2.702(1)	142.0	-x, -y, ½ +z

while the other axial site is coordinated to a thiocyanate ligand. The axial Co-O(H_2O) bond distance (2.157 Å) is slightly longer than the Co-O(H_2O) bond distance (2.135 Å) of the precursor complex. The Co-N(thiocyanato) bond distance (2.073 Å) is slightly shorter than the Co-N(thiocyanato) bond distances of compounds **6** and **7**. The coordinated and lattice molecules present the mononuclear PBP Co(II) compounds **5-10** participate in the formation of interesting hydrogen bonding architectures. All the structural parameters of hydrogen bonds are listed in Table 3.4.

Hydrogen bonding pattern present in compound **5** is depicted in Figure 3.8. Both the axial H_2O molecules attached to the central Co(II) atom of compound **5** are involved in the formation of extensive hydrogen bonding. One of the axial water molecules, O(3) is hydrogen bonded to the O(1) oxygen atom of the bis-hydrazone ligand H_2L. The other axial water molecule, O(4) attached to the central Co(II) atom is hydrogen bonded to the oxygen atom of the nitrate group present in the coordination sphere through O(4)-H(4B)¨O(9) linkage. The lattice water molecules present are hydrogen bonded to each other. This eventually gives rise to a two dimensional network through the formation of a H-bonded 10-membered ring.

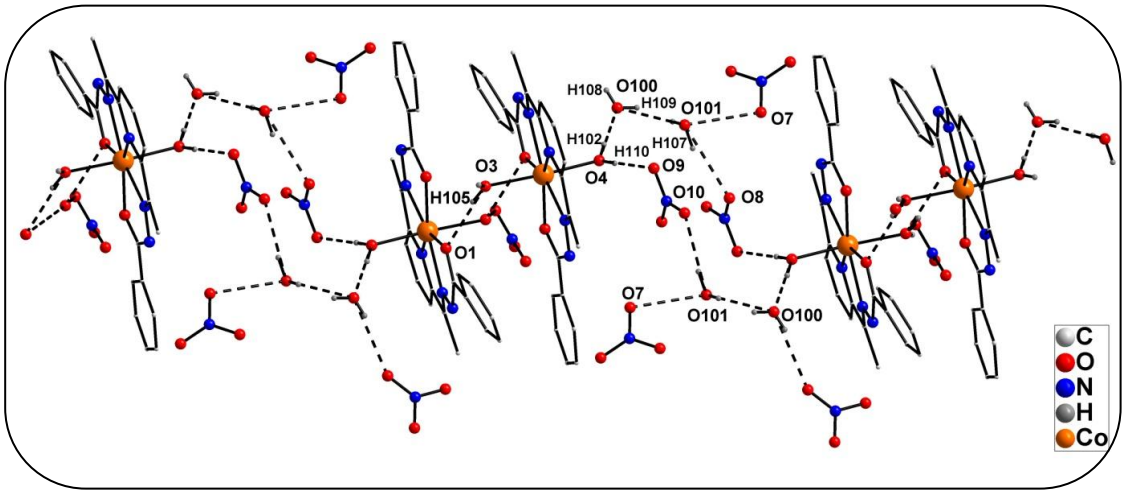

Figure 3.8. Hydrogen bonding network present in compound **5**

In compound **7**, extensive hydrogen bonding networks involving the lattice water molecules are observed. The hydrogen bonding pattern in compound **7** is shown in Figure 3.9. The lattice water molecules present in compound **7** gives rise to an interesting hydrogen bonding pattern. One of the lattice water molecule O(4) is hydrogen bonded to the two oxygen atoms O(1) and O(2) of the bis hydrazone moiety. The other lattice water molecules are hydrogen bonded to the two sulphur atoms of the

axial thiocyanate units through O(5)-H(5A)···S(1) and O(6)-H(6A)···S(2) bonds. This criss-cross hydrogen bonding gives rise to the formation of a one dimensional chain like structure as shown in Figure 3.9.

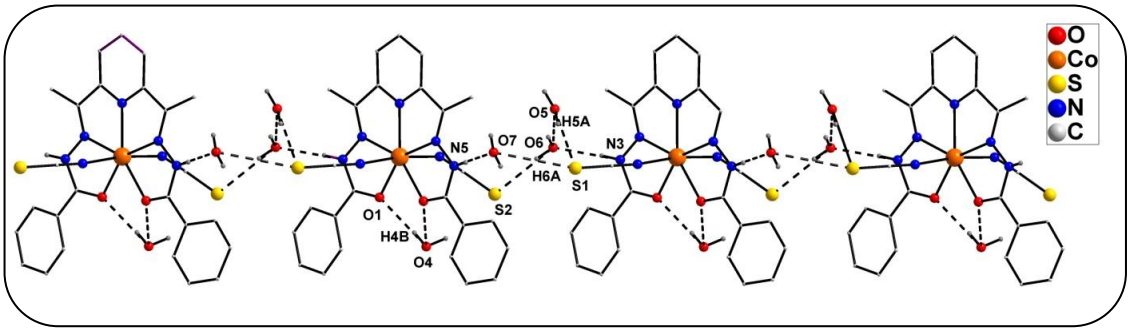

Figure 3.6. Hydrogen bonding network present in compound **7**

Compound **8** also features interesting hydrogen bonding pattern as shown in Figure 3.10. Only the oxygen atom O(3) of the coordinated water molecule participate in intermolecular hydrogen bonding with the oxygen atoms, O(1) and O(2) of the bis hydrazone ligand through O(3)-H(3A)···O(1)/O(2) hydrogen bonds. This leads to the formation of a dimeric structure as depicted in Figure 3.10. The two monomeric units participating in intermolecular hydrogen bonding are arranged in alternate fashion giving rise to a trans arrangement of the units.

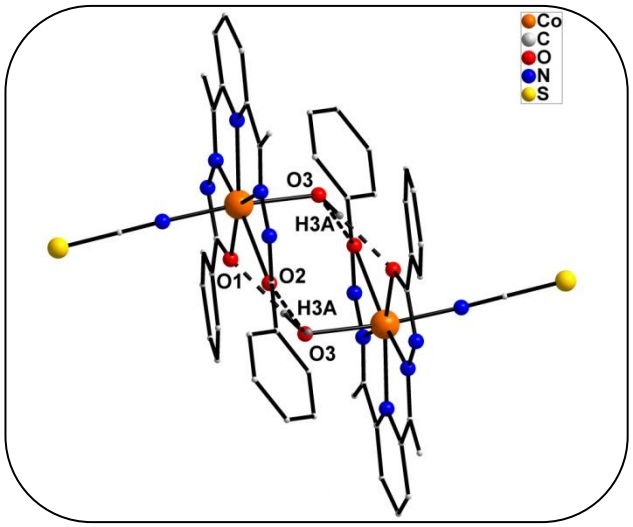

Figure 3.10. Hydrogen bonding network present in compound **8**

The hydrogen bonding pattern formed by the lattice molecules in compound **9** has been depicted in Figure 3.11. Each asymmetric unit possesses a nitrate group and a water

molecule. These two groups are involved in extensive hydrogen bonding network with the lattice molecules of the nearby unit. One of the oxygen atom of the nitrate group O(103) is hydrogen bonded to another oxygen atom O(4) of the water molecule attached to one of the axial sites of the PBP Co(II) center. The nitrogen atom N(5) of the imine group of the bis-hydrazone ligand H_2L is hydrogen bonded to the oxygen atom O(100) of the lattice water molecule through N(5)-H(5)···O(100) linkage. Thus, hydrogen bonding between the two nitrate groups and two water molecules leads to the formation of a cyclic tetramer throughout the chain.

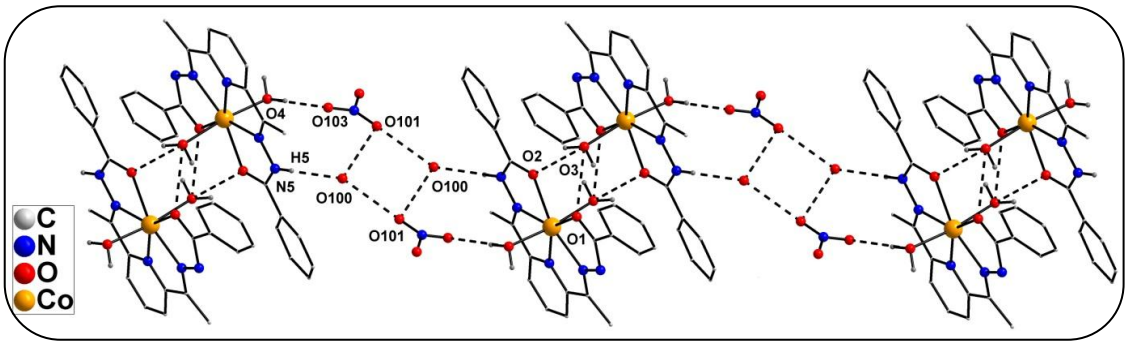

Figure 3.11. Hydrogen bonding network present in compound **9**

In compound **10**, both the axial water molecules of the PBP Co(II) center are hydrogen bonded to the two oxygen atoms of the bis hydrazone moiety of the ligand L present in the consecutive units. Each mononuclear Co(II) units are packed in a alternate fashion to each other. This arrangement is responsible for the formation of a one dimensional chain like pattern throughout the crystal lattice as shown in Figure 3.12.

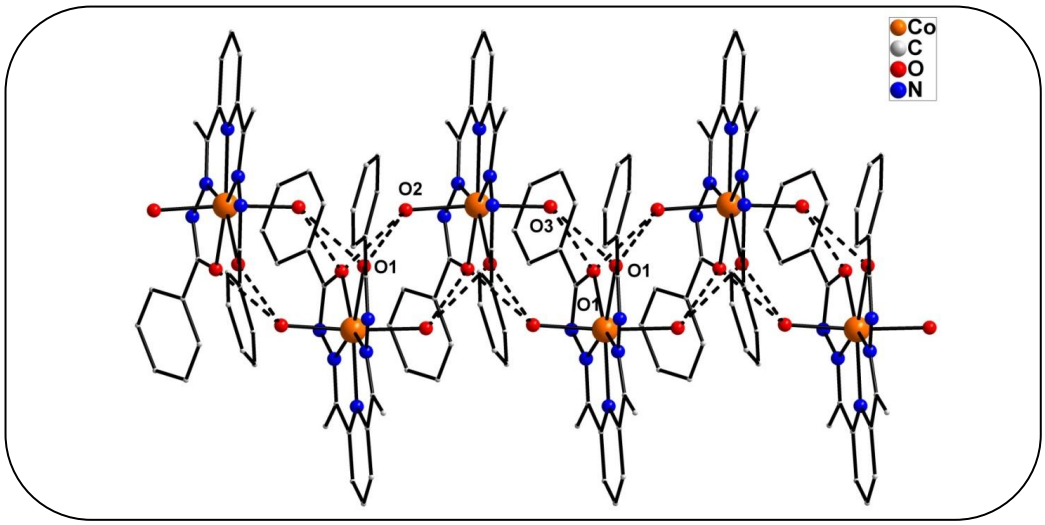

Figure 3.12. Hydrogen bonding network present in compound **10**

3.3.7. Superoxide dismutase activity

The superoxide scavenging activity of the mononuclear Co(II) compounds **5-10** were investigated by employing a modified nitro blue tetrazolium (NBT) assay. The indirect determination of SOD activity was monitored by the reduction of NBT by superoxide generated by alkaline DMSO. As the reaction proceeds, the colour of the resulting solution changes from light yellow to blue due to the formation of blue formazan which can be detected spectrophotometrically.

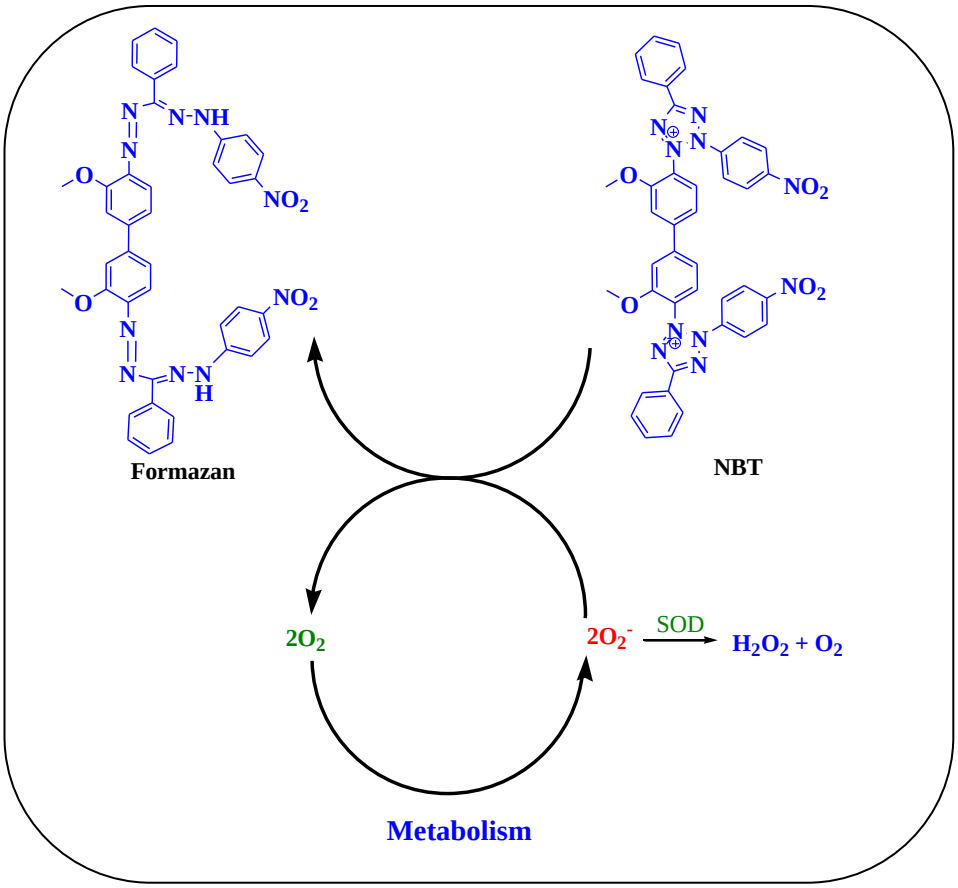

Scheme 3.6. Probable mechanism for the reduction of NBT by superoxide

Compounds **5**, **9** and **10** are catalytically active towards superoxide dismutase whereas the other mononuclear Co(II) compounds do not show any superoxide dismutase activity. The IC_{50} values of the compounds **5**, **9** and **10** are calculated to be 3.5, 3.6 and 4.0 µM respectively (Figure 3.13). These values signify that compound **5** acts as a better SOD mimic than the other two compounds. This further confirms that the presence of labile aqua-ligands in the axial coordination of the metal complexes is the essential criteria for the SOD catalysis by these compounds.

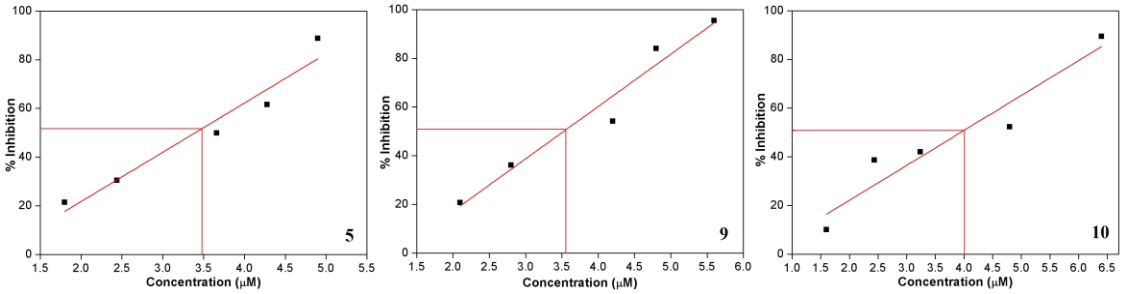

Figure 3.13. Determination of IC_{50}: Inhibition percentage as a function of the concentrations of compounds **5**, **9** and **10** respectively

Table 3.5. IC_{50} values of mononuclear PBP Co(II) complexes

Sl.No.	Complexes	IC_{50} value	References
1.	Native MnSOD	0.005	50
2.	$[Co(H_2L)(H_2O)_2](NO_3).2H_2O$ (**5**)	3.5	This work
3.	$[Co(H_2L)(SCN)_2].3H_2O$ (**6**)	Not active	This work
4.	$[Co(H_2L)(SCN)_2].4H_2O$ (**7**)	Not active	This work
5.	$[Co(HL)(H_2O)(SCN)]$ (**8**)	Not active	This work
6.	$[Co(HL)(H_2O)_2](NO_3).H_2O$ (**9**)	3.6	This work
7.	$[Co(L)(H_2O)_2]$ (**10**)	4.0	This work

H_2L: 2,6-diacetylpyridine bis(benzoyl hydrazone)

3.3.8. Variable temperature magnetic studies of compounds 5-10

Magnetization studies on polycrystalline samples of **5-10** were performed under a constant static field of 1000 Oe between 2-300 K. Figure 3.14 depicts the variation of $\chi_M T$ between 2-300 K for compounds **5-10** respectively. The expected $\chi_M T$ product for a magnetically isolated Co(II) center considering S= 3/2 and g = 2.0 is 1.875 cm^3Kmol^{-1}. However at 300 K, the $\chi_M T$ product for all the mononuclear Co(II) compounds are found to be 1.86, 2.11, 1.85, 1.99 and 1.93 cm^3Kmol^{-1} for compounds **5-10** respectively. On lowering the temperature, $\chi_M T$ product does not change appreciably until about 55 K for all the mononuclear Co(II) compounds. However, on further cooling, $\chi_M T$ drops abruptly to reach a minimum of 1.51, 1.43 and 0.96, 1.54 and 1.01 cm^3Kmol^{-1} for compounds **5-10** respectively. Deviation of $\chi_M T$ product from the expected value and its rapid decrease at low temperature regime indicate the presence of significant orbital magnetic moment in mononuclear PBP Co(II) complexes. Good quality fitting of the temperature dependence of $\chi_M T$ plots of all the compounds are

obtained by using PHI program and it yields g = 2.16, 2.13, 2.17, 2.06 and 2.06 for complexes **5-10** respectively.

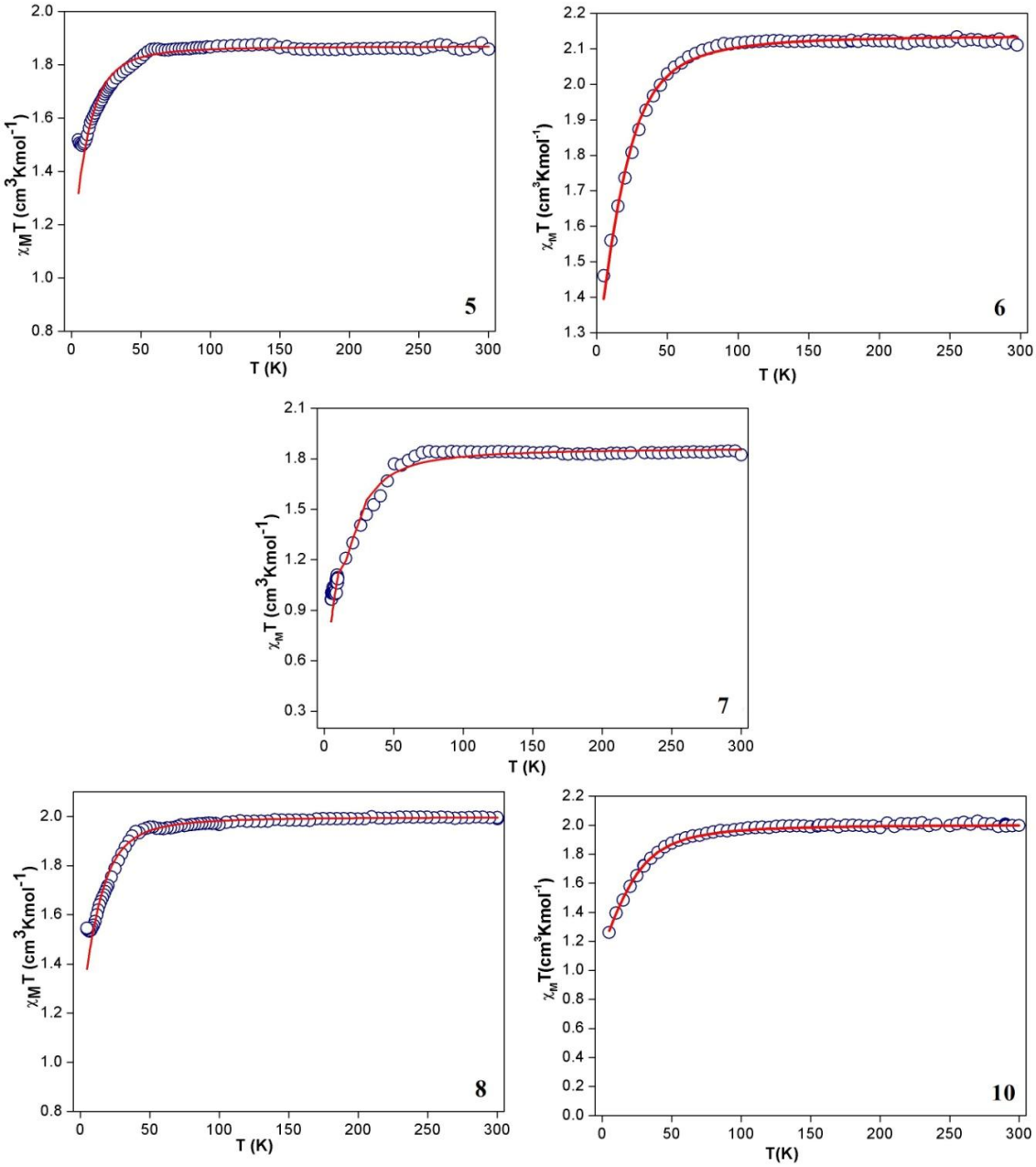

Figure 3.14. Temperature dependence of $\chi_M T$ between 2-300 K for compounds **5-10** respectively. The circles represent experimental data and the solid lines indicate the best fit obtained by using PHI program

Temperature dependence of $1/\chi_M$ of compounds **5-10** between 2-300 K is depicted in Figure 3.15. Curie-Weiss law is obeyed by all the compounds with a Weiss constant θ = 1.78 K, 1.79 K, 1.67 K, 1.34 K and 1.54 K for complexes **5-10** respectively. The

Weiss constant bears a positive sign for all the complexes, which clearly indicates that ferromagnetic interactions between the spin carriers are operative in compounds **5-10**.The Curie constant C are found to lie between 1.69-1.98 cm^3Kmol^{-1} and the values of C obtained experimentally for compounds **5-10** are in good agreement with the calculated C value of 1.875 cm^3Kmol^{-1} for an isolated high spin Co(II) center with S=3/2 assuming g_{Co}=2.0.

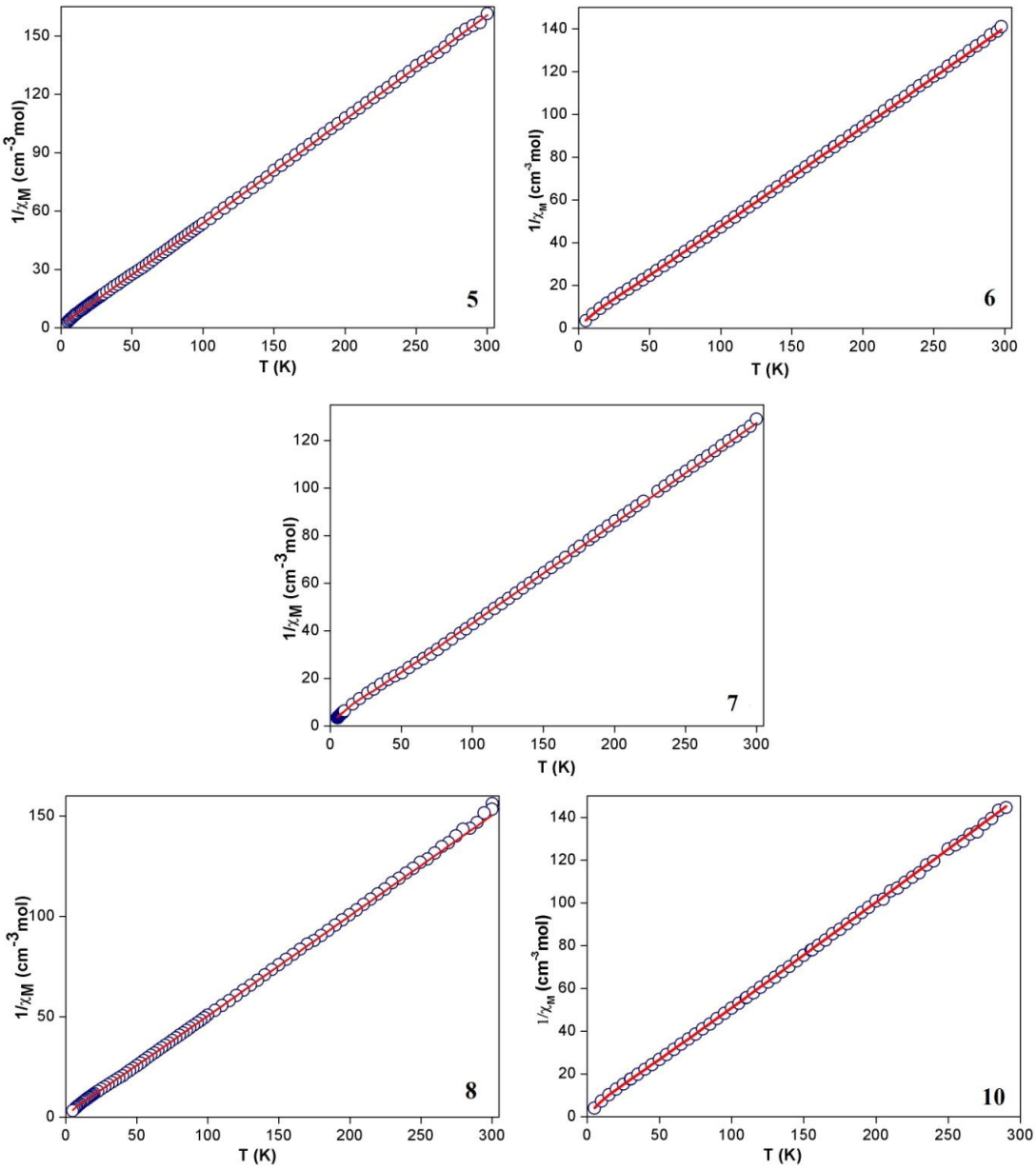

Figure 3.15. Variation of $1/\chi_M$ against temperature for compounds **5-10**. Circles represent experimental value and the solid line represents the best fit obtained by using PHI program

Isothermal field dependence of magnetization measurements of compounds **5-10** were performed between 0-5 T at temperature range of 2-10 K. The reduced magnetization plots of compounds **5-10** at different temperatures are depicted Figure 3.16. The reduced magnetization plots at different temperatures for all the compounds do not superimpose on each other. The above observations unambiguously establish the presence of significant magnetic anisotropy in the mononuclear PBP Co(II) compounds **5-10**.

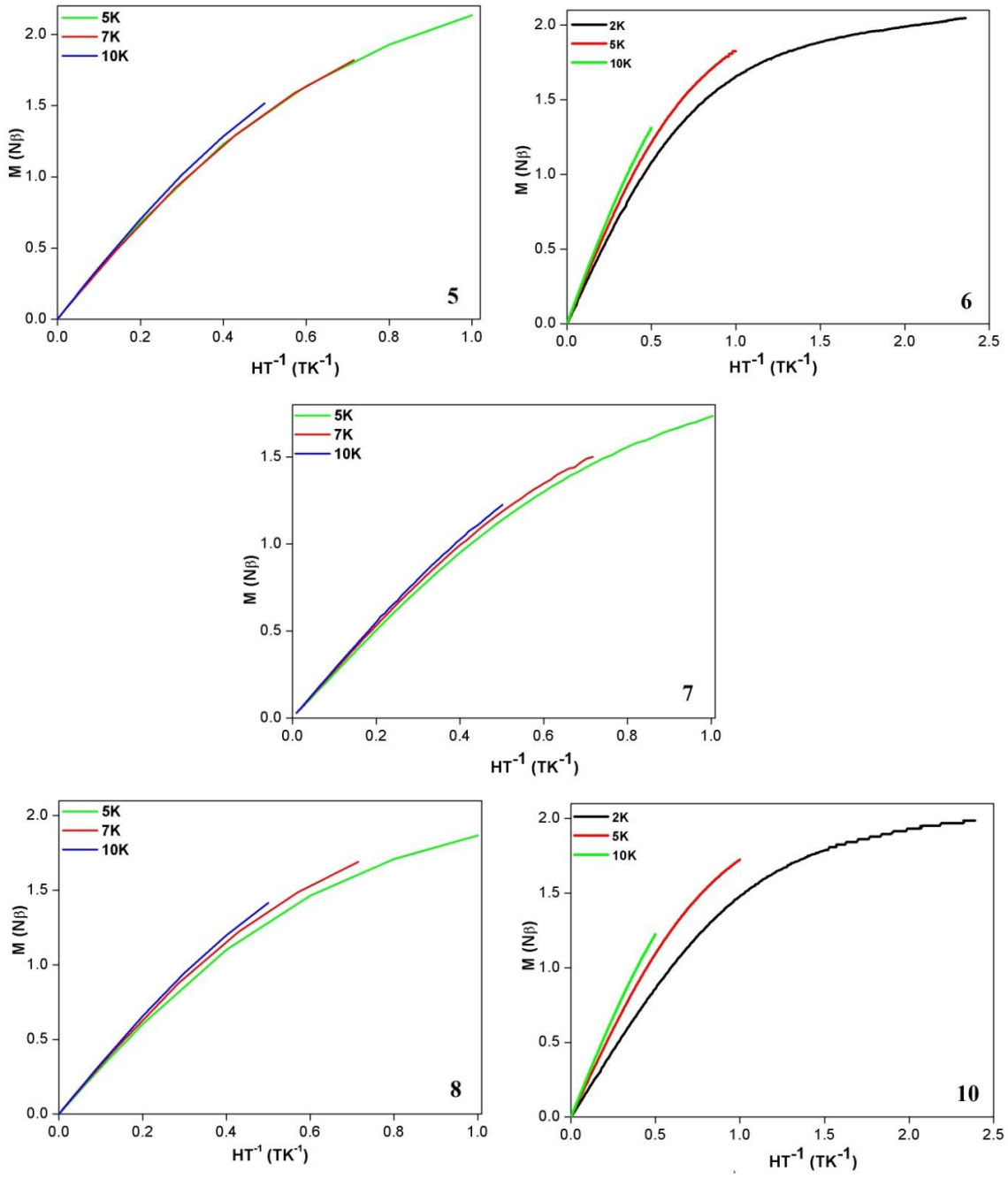

Figure 3.16. Reduced magnetization plots of compounds **5-10** respectively

The field dependence of magnetization for compounds **5-10** at 2 K, 5 K, 7 K and 10 K along with the calculated value for 2 K for an isotropic system has been depicted in Figure 3.17. Although with increase of field strength, magnetization increases linearly initially, saturation magnetization M_s = 3 μB (for S = 3/2 and g = 2.0) was not achieved

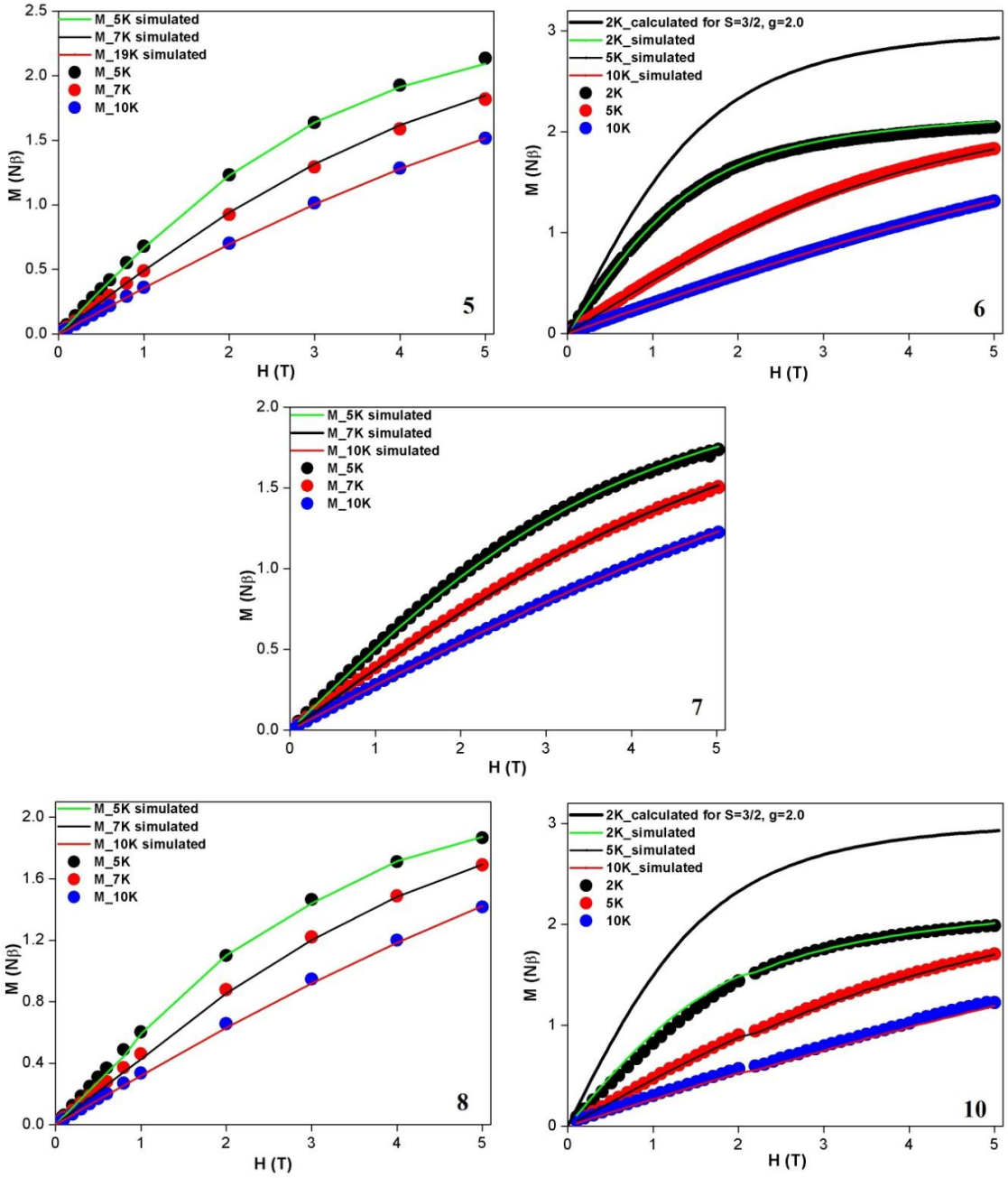

Figure 3.17. Field dependence of magnetization between 0-5 T for compounds **5-10** respectively along with the calculated magnetization behaviour for an isotropic S=3/2 system. Circles represent experimental value and the solid lines are the best fit obtained by using PHI program

even at a field strength of 5 T. Moreover, the calculated magnetization behaviour for an isotropic S=3/2 system at 2 K deviated considerably from the experimental magnetization behaviour in all the cases.

A spin Hamiltonian ($\hat{H}$) of equation 1 can be utilized to qualitatively describe magnetic anisotropy:

$$\hat{H} = D[S_z^2 - S(S+1)/3] + E(S_x^2 - S_y^2) + g\beta SB + AIS \qquad (1)$$

where β, E, S and B represent Bohr magneton, rhombic ZFS parameter, spin and magnetic field vectors and AIS is the nuclear hyperfine splitting term respectively. The best fits of the field dependant magnetization plots of compounds **5-10** obtained by using PHI program yields D = 13.46 cm^{-1}, 15.9 cm^{-1}, 6.19 cm^{-1}, 7.09 cm^{-1} and 13.1 cm^{-1} respectively for complexes **5-10** respectively. The D values obtained for all the compounds are significantly lower than the D values reported for other PBP Co(II) complexes (Chart 3.1).

Table 3.6. Data obtained from ORCA program for compounds **5-10**

Complex	$\mathbf{D_{exp}}$	$\mathbf{D_{calc}}$	**E/D**	$\mathbf{Dss_C}$	$\mathbf{D_{SOC}}$	**α→α**	**β→β**	**α→β**	**β→α**
5	13.46	10.17	0.0072	1.764	8.403	0.002	5.151	3.264	-0.014
6	15.9	15.09	0.0102	2.364	12.741	0.039	9.497	3.252	-0.047
7	6.19	5.03	0.0480	0.928	4.102	0.001	1.623	2.486	-0.008
8	7.09	8.02	0.0396	1.669	6.352	0.080	3.068	3.234	-0.030
9	-	12.04	0.0151	2.060	9.965	0.017	6.427	3.539	-0.019
10	13.1	12.48	0.0925	2.235	10.251	1.196	5.981	4.203	-1.128

The smaller positive D values observed in compounds **5-10** in comparison to other reported PBP Co(II) complexes can be explained in light of theoretical calculations performed earlier. It is well established that the large positive D parameter in PBP Co(II) complexes originates from spin-orbit mixing of the ground quartet state with three excited state, two being quartets and the other is a doublet [47]. The quartet excited state with highest contribution to D represents an electronic configuration obtained by promoting an electron from the d_{xz} or d_{yz} orbital to the d_z^2 orbital (Figure 3.18). On increasing the energy of the d_z^2 orbital by employing better σ-donor apical ligands, the spin-orbit interaction between the ground quartet state with this excited quartet state is reduced. Thus the better σ-donor apical ligands in compound **6** and **7**

reduce the positive D parameter by reducing the contribution of second order perturbation in spin orbit coupling.

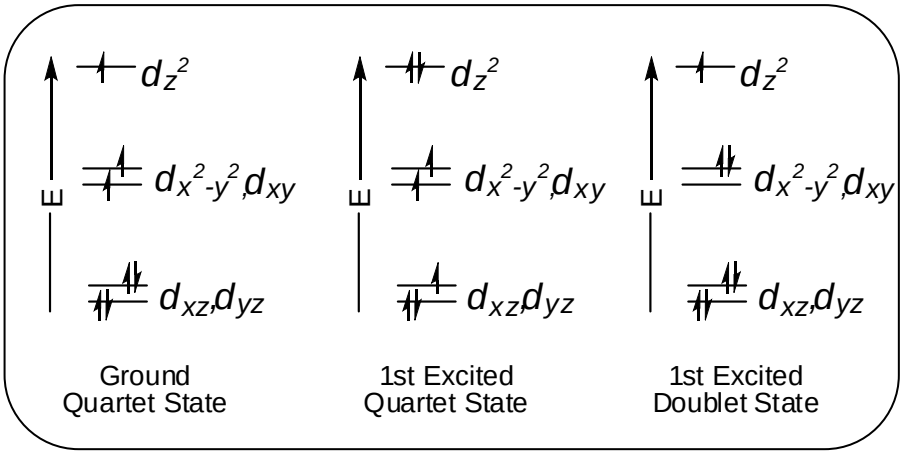

Figure 3.18. Electronic arrangement in the ground quartet, 1st excited quartet and 1st excited doublet states

Another important contribution to the positive D parameter in PBP Co(II) complexes arise from spin orbit mixing of the ground quartet with an excited doublet state. This doublet excited state refers to an electronic state obtained by either promoting an electron from d_{xy} to $d_{x^2-y^2}$ orbital or from $d_{x^2-y^2}$ to d_{xy} orbital (Figure 3.18). The energy gap between the d_{xy} and $d_{x^2-y^2}$ reduces when a symmetric equatorial field is applied. The bis-hydrazone ligand in compound **10** is in dianionic form and both the anionic charges are conjugated. Further, the metal-donor atom bond distances within the equatorial plane are found to be relatively shorter as compared to bond distances reported for other Co-H_2L complexes. Therefore, the conjugated anionic bis-hydrazone ligand enforces a strong equatorial ligand field environment in compound **10** and the excited doublet state is expected to lie at higher energy. Moreover, due to the presence of C_2 symmetry, the equatorial ligand, H_2L is structurally symmetric. This enforces a more symmetric equatorial coordination environment as compared to neutral H_2L ligand while the d_{xy} and $d_{x^2-y^2}$ lie within a narrow energy gap. Consequently, the positive contribution to D parameter originating from spin-orbit interaction of ground quartet state with excited doublet state is reduced in compound **10**.

The bis-hydrazone ligand is in mono-anionic form in case of compound **8** and **9** and this explains the lower D values observed in these compounds. Further, one of the axial sites in compound **8** is occupied by stronger σ-donor ligand, SCN^- and therefore the D

values observed in compound **8** is reasonably smaller as compared to that calculated for compound **9**. In case of compound **5**, the bis-hydrazone ligand is in neutral form and both the axial sites are occupied by H_2O, a poor σ-donor ligand. Therefore, the D value of compound **5** is expected to be considerably large as compared to the other mononuclear PBP Co(II) complexes reported herein. However, the D value observed for compound **5** is comparable to the D value observed in case of compound **6**, where both the axial sites are occupied by SCN^- ligand.

Careful analysis of the crystal structures of all the compounds revealed that equatorial Co-O bond distances are reasonably shorter in case of compound **5** as compared to those observed in all other Co(II) compounds. Moreover, all other equatorial bond distances in compound **5** are comparable to those observed in other Co(II) compounds. Thus, the short equatorial Co-O bond distances in compound **5** implies interplay of a strong equatorial ligand field environment and this could be attributed to the lower D value observed in compound **5**. Intriguingly, the ZFS values of compounds **6** and **7**, which have identical coordination environment, differ by a considerably large extent. This anomaly in ZFS parameters within the complexes of identical coordination environment can be explained with the help of symmetry consideration around Co(II) centers. SHAPE analysis of the compounds **6** and **7** have revealed that the deviation of local coordination geometry around Co(II) center from ideal PBP geometry reasonably highest for compound **7**. Deviation of the local coordination geometry from ideal PBP geometry increases the difference in energy between the d_{xz} and d_{yz} orbitals. Thus, decrease in symmetry reduces the orbital degeneracy of the 1^{st} excited quartet state. Quenching of orbital angular momentum of excited state leads to eventual decrease in SOC and therefore the D values observed in compound **7** is considerably smaller than that observed in compound **6**.

3.4. Conclusions

Reaction of the precursor complex $[Co(H_2L)(H_2O)(NO_3)]NO_3$ with various ligands yielded six novel compounds, $[Co(H_2L)(H_2O)_2](NO_3)_2.2H_2O$ (**5**), $[Co(H_2L)(SCN)_2].3H_2O$ (**6**), $[Co(H_2L)(SCN)_2].4H_2O$ (**7**), $[Co(HL)(SCN)(H_2O)]$ (**8**), $[Co(HL)(H_2O)_2](NO_3).H_2O$ (**9**) and $[Co(L)(H_2O)_2]$ (**10**) in good yield. The synthesized compounds have been characterized using various analytical and spectroscopic studies and single crystal X-ray diffraction study was carried out to completely elucidate its

structure in the solid state. All the six compounds possess different coordination environments. The bis hydrazone ligand in compounds **5**, **6** and **7** are in neutral form, while in compounds **8** and **9**, it is in monoanionic form. Compound **10** possesses a dianionic form of the bis-hydrazone ligand. The magnetization studies of these compounds have been performed to determine the ZFS parameters. Results presented herein support earlier theoretical findings that the second order spin-orbit perturbation mediated control of magnetic anisotropy is possible by appropriate modulation of coordination environment [46]. It is observed that either by employing a strong σ-donor apical ligand or by using a symmetric pentadentate equatorial ligand, it is possible to significantly decrease the positive contribution to D parameter. Earlier approaches to modulate axial ZFS parameter through modification of coordination environment primarily relied on covalent character of metal-ligand linkages [47]. However, for PBP Co(II)-H_2L complexes reported so far no such trend based on hard/soft character of the donor ligands is observed [46]. Instead, the present approach of modulating magnetic anisotropy is based on tuning the contribution of second order perturbation to spin-orbit coupling in a predetermined fashion by modifying the energy of the excited levels. However, deviation from the ideal PBP geometry also induces the variation of the D value. More the compound is deviated from the ideal PBP geometry, lower is the D value observed for the PBP Co(II) complexes. Thus, even in high coordinate species with no first order perturbation to magnetic anisotropy there is a possibility to induce magnetic anisotropy by appropriately modulating the coordination environment. Proliferation of the present approach is anticipated to open fascinating frontiers for synthetic chemist to induce magnetic anisotropy in high coordinate species.

3.5. References

[1] Neese, F., and Pantazis, D. A. What is not required to make a single molecule magnet. *Faraday Discussions*, 148: 229-238, 2011.

[2] Waldmann, O. A criterion for the anisotropy barrier in single-molecule magnets. *Inorganic Chemistry*, 46(24): 10035-10037, 2007.

[3] Dey, M., and Gogoi, N. Geometry-Mediated Enhancement of Single-Ion Anisotropy: A Route to Single-Molecule Magnets with a High Blocking Temperature. *Angewandte Chemie International Edition*, 52(49): 12780-12782, 2013.

[4] Ruiz, E., Cirera, J., Cano, J., Alvarez, S., Loose, C., and Kortus, J. Can large magnetic anisotropy and high spin really coexist?. *Chemical Communications*, (1): 52-54, 2008.

[5] Bar, A. K., Pichon, C., and Sutter, J. P. Magnetic anisotropy in two-to eight-coordinated transition–metal complexes: Recent developments in molecular magnetism. *Coordination Chemistry Reviews*, 308: 346-380, 2016.

[6] Blagg, R.J., Muryn, C.A., McInnes, E.J., Tuna, F. and Winpenny, R.E. Single pyramid magnets: Dy_5 pyramids with slow magnetic relaxation to 40 K. *Angewandte Chemie International Edition*, 50(29): 6530-6533, 2011.

[7] Rinehart, J. D., Fang, M., Evans, W. J., and Long, J. R. Strong exchange and magnetic blocking in N_2^{3-}-radical-bridged lanthanide complexes. *Nature Chemistry*, 3(7): 538-542, 2011.

[8] Rinehart, J. D., Fang, M., Evans, W. J., and Long, J. R. A N_2^{3-} Radical-Bridged Terbium Complex Exhibiting Magnetic Hysteresis at 14 K. *Journal of the American Chemical Society*, 133(36): 14236-14239, 2011.

[9] Meihaus, K. R., and Long, J. R. Magnetic blocking at 10 K and a dipolar-mediated avalanche in salts of the bis (η^8-cyclooctatetraenide) complex $[Er(COT)_2]^-$. *Journal of the American Chemical Society*, 135(47): 17952-17957, 2013.

[10] Le Roy, J. J., Ungur, L., Korobkov, I., Chibotaru, L. F., and Murugesu, M. Coupling Strategies to Enhance Single-Molecule Magnet Properties of Erbium–Cyclooctatetraenyl Complexes. *Journal of the American Chemical Society*, 136(22): 8003-8010, 2014.

[11] Ungur, L., Le Roy, J. J., Korobkov, I., Murugesu, M., and Chibotaru, L. F. Fine-tuning the Local Symmetry to Attain Record Blocking Temperature and Magnetic Remanence in a Single-Ion Magnet. *Angewandte Chemie International Edition*, 53(17): 4413-4417, 2014.

[12] Ishikawa, N., Sugita, M., Ishikawa, T., Koshihara, S. Y., and Kaizu, Y. Lanthanide double-decker complexes functioning as magnets at the single-molecular level. *Journal of the American Chemical Society*, 125(29): 8694-8695, 2003.

[13] Rinehart, J. D., and Long, J. R. Exploiting single-ion anisotropy in the design of f-element single-molecule magnets. *Chemical Science*, 2(11): 2078-2085, 2011.

[14] Jiang, S. D., Wang, B. W., Sun, H. L., Wang, Z. M., and Gao, S. An organometallic single-ion magnet. *Journal of the American Chemical Society*, 133(13): 4730-4733, 2011.

[15] Gómez-Coca, S., Aravena, D., Morales, R., and Ruiz, E. Large magnetic anisotropy in mononuclear metal complexes. *Coordination Chemistry Reviews*, 289: 379-392, 2015.

[16] Boča, R. Zero-field splitting in metal complexes. *Coordination Chemistry Reviews*, 248(9): 757-815, 2004.

[17] Zadrozny, J. M., Atanasov, M., Bryan, A. M., Lin, C. Y., Rekken, B. D., Power, P. P., and Long, J. R. Slow magnetization dynamics in a series of two-coordinate iron (II) complexes. *Chemical Science*, 4(1): 125-138, 2013.

[18] Zadrozny, J. M., Xiao, D. J., Long, J. R., Atanasov, M., Neese, F., Grandjean, F., and Long, G. J. Mössbauer Spectroscopy as a Probe of Magnetization Dynamics in the Linear Iron (I) and Iron (II) Complexes $[Fe(C(SiMe_3)_3)_2]^{1-/0}$. *Inorganic chemistry*, 52(22): 13123-13131, 2013.

[19] Poulten, R. C., Page, M. J., Algarra, A. G., Le Roy, J. J., López, I., Carter, E., Llobet, A., Macgregor, S. A., Mahon, M.F., Murphy, D. M. and Murugesu, M. Synthesis, electronic structure, and magnetism of $[Ni(6\text{-}Mes)_2]^+$: A two-coordinate nickel (I) complex stabilized by bulky N-heterocyclic carbenes. *Journal of the American Chemical Society*, 135(37): 13640-13643, 2013.

[20] Zadrozny, J. M., Xiao, D. J., Atanasov, M., Long, G. J., Grandjean, F., Neese, F., and Long, J. R. Magnetic blocking in a linear iron (I) complex. *Nature Chemistry*, 5(7): 577-581, 2013.

[21] Bartolomé, E., Alonso, P. J., Arauzo, A., Luzón, J., Bartolomé, J., Racles, C., and Turta, C. Magnetic properties of the seven-coordinated nanoporous framework material $Co(bpy)_{1.5}(NO_3)_2$ (bpy=4,4′-bipyridine). *Dalton Transactions*, 41(34): 10382-10389, 2012.

[22] Platas-Iglesias, C., Vaiana, L., Esteban-Gómez, D., Avecilla, F., Real, J. A., de Blas, A., and Rodríguez-Blas, T. Electronic structure study of seven-coordinate first-row transition metal complexes derived from 1, 10-diaza-15-crown-5: A successful marriage of theory with experiment. *Inorganic Chemistry*, 44(26): 9704-9713, 2005.

[23] Schleife, F., Rodenstein, A., Kirmse, R., and Kersting, B. Seven-coordinate Mn(II) and Co(II) complexes of the pentadentate ligand 2,6-diacetyl-4-carboxymethyl-pyridine bis (benzoylhydrazone): Synthesis, crystal structure and magnetic properties. *Inorganica Chimica Acta*, 374(1): 521-527, 2011.

[24] Drahoš, B., Herchel, R., and Trávníček, Z. Structural, Magnetic, and Redox Diversity of First-Row Transition Metal Complexes of a Pyridine-Based Macrocycle: Well-Marked Trends Supported by Theoretical DFT Calculations. *Inorganic Chemistry*, 54(7): 3352-3369, 2015.

[25] Venkatakrishnan, T. S., Sahoo, S., Bréfuel, N., Duhayon, C., Paulsen, C., Barra, A. L., Ramasesha, S., and Sutter, J. P. Enhanced ion anisotropy by nonconventional coordination geometry: single-chain magnet behavior for a $[\{Fe^{II}L\}_2\{Nb^{IV}(CN)_8\}]$ helical chain compound designed with heptacoordinate Fe^{II}. *Journal of the American Chemical Society*, 132(17): 6047-6056, 2010.

[26] Bar, A. K., Pichon, C., Gogoi, N., Duhayon, C., Ramasesha, S., and Sutter, J. P. Single-ion magnet behaviour of heptacoordinated Fe(II) complexes: on the importance of supramolecular organization. *Chemical Communications*, 51(17): 3616-3619, 2015.

[27] Ruamps, R., Batchelor, L.J., Maurice, R., Gogoi, N., Jiménez-Lozano, P., Guihéry, N., de Graaf, C., Barra, A.L., Sutter, J.P. and Mallah, T. Origin of the magnetic anisotropy in heptacoordinate Ni^{II} and Co^{II} complexes. *Chemistry-A European Journal*, 19(3): 950-956, 2013.

[28] Huang, X. C., Zhou, C., Shao, D., and Wang, X. Y. Field-Induced Slow Magnetic Relaxation in Cobalt (II) Compounds with Pentagonal Bipyramid Geometry. *Inorganic Chemistry*, 53(24): 12671-12673, 2014.

[29] Batchelor, L. J., Sangalli, M., Guillot, R., Guihéry, N., Maurice, R., Tuna, F., and Mallah, T. Pentanuclear cyanide-bridged complexes based on highly anisotropic coii seven-coordinate building blocks: synthesis, structure, and magnetic behavior. *Inorganic Chemistry*, 50(23): 12045-12052, 2011.

[30] Antal, P., Drahoš, B., Herchel, R., and Trávníček, Z. Late First-Row Transition-Metal Complexes Containing a 2-Pyridylmethyl Pendant-Armed 15-Membered Macrocyclic Ligand. Field-Induced Slow Magnetic Relaxation in a Seven-Coordinate Cobalt (II) Compound. *Inorganic Chemistry*, 55 (12): 5957-5972, 2016.

[31] Drahoš, B., Herchel, R., and Trávníček, Z. Structural, Magnetic, and Redox Diversity of First-Row Transition Metal Complexes of a Pyridine-Based Macrocycle: Well-Marked Trends Supported by Theoretical DFT Calculations. *Inorganic Chemistry*, 54(7): 3352-3369, 2015.

[32] Batchelor, L. J., Sangalli, M., Guillot, R., Guihéry, N., Maurice, R., Tuna, F., and Mallah, T. Pentanuclear cyanide-bridged complexes based on highly anisotropic coii seven-coordinate building blocks: synthesis, structure, and magnetic behavior. *Inorganic Chemistry*, 50(23): 12045-12052, 2011.

[33] Chen, L., Chen, S. Y., Sun, Y. C., Guo, Y. M., Yu, L., Chen, X. T., Wang, Z., Ouyang, Z. W., Song, Y., and Xue, Z. L. Slow magnetic relaxation in mononuclear seven-coordinate cobalt (II) complexes with easy plane anisotropy. *Dalton Transactions*, 44(25): 11482-11490, 2015.

[34] Vaidya, S., Upadhyay, A., Singh, S.K., Gupta, T., Tewary, S., Langley, S.K., Walsh, J.P., Murray, K.S., Rajaraman, G. and Shanmugam, M. A synthetic strategy for switching the single ion anisotropy in tetrahedral Co (II) complexes. *Chemical Communications*, 51(18): 3739-3742, 2015.

[35] Giordano, T. J., Palenik, G. J., Palenik, R. C., and Sullivan, D. A. Pentagonal-bipyramidal complexes. Synthesis and characterization of aqua (nitrato)[2,6-diacetylpyridine bis (benzoyl hydrazone)] cobalt (II) nitrate and diaqua [2,6-diacetylpyridine bis (benzoyl hydrazone)] nickel (II) nitrate dihydrate. *Inorganic Chemistry*, 18(9) 2445-2450, 1979.

[36] Villanueva, M., Urtiaga, M.K., Mesa, J.E.L. and Arriortua, M.I. Diazidobis (2, 2′-dipyridylamine) nickel(II) monohydrate. *Acta Crystallographica Section E: Structure Reports Online*, 60(8): m1175-m1177, 2004.

[37] Bhirud, R. G., and Srivastava, T. S. Synthesis, characterization and superoxide dismutase activity of some ternary copper (II) dipeptide-2, 2′-bipyridine, 1,10-phenanthroline and 2,9-dimethyl-1,10-phenanthroline complexes. *Inorganica Chimica Acta*, 179(1): 125-131, 1991.

[38] Bhirud, R. G., and Srivastava, T. S. Superoxide dismutase activity of $Cu(II)_2(aspirinate)_4$ and its adducts with nitrogen and oxygen donors. *Inorganica Chimica Acta*, 173(1): 121-125, 1990.

[39] Sheldrick, G. M. A short history of SHELX. *Acta Crystallographica Section A: Foundations of Crystallography*, 64(1): 112-122, 2008.

[40] Llunell, M., Casanova, D., Cirera, J., Bofill, J. M., Alemany, P., Alvarez, S., Pinsky, M. and Avnir, D. *SHAPE: Continuous shape measures of polygonal and polyhedral molecular fragments*; University of Barcelona: Barcelona, 2005.

[41] Neese, F. *ORCA - an ab initio, Density Functional and Semiempirical Program Package*; University of Bonn, Germany, 2007.

[42] Andrae, D., Haeussermann, U., Dolg, M., Stoll, H., and Preuss, H. Energy-adjustedab initio pseudopotentials for the second and third row transition elements. *Theoretica chimica acta*, 77(2): 123-141, 1990.

[43] Schäfer, A., Huber, C., and Ahlrichs, R. Fully optimized contracted Gaussian basis sets of triple zeta valence quality for atoms Li to Kr. *The Journal of Chemical Physics*, 100(8): 5829-5835, 1994.

[44] Becke, A. D. A new mixing of Hartree–Fock and local density-functional theories. *The Journal of Chemical Physics*, 98(2): 1372-1377, 1993.

[45] Dey, M., Sarma, B. and Gogoi, N. Coligand Promoted Controlled Assembly of Hierarchical Heterobimetallic Nitroprusside Based Aggregates. *Zeitschrift für Anorganische und Allgemeine Chemie*, 640(14): 2962-2967, 2014.

[46] Konar, S., Jana, A., Das, K., Ray, S., Chatterjee, S., Golen, J. A., Rheingold, A. L., & Kar, S. K. Synthesis, crystal structure, spectroscopic and photoluminescence studies of manganese (II), cobalt (II), cadmium (II), zinc (II) and copper (II) complexes with a pyrazole derived Schiff base ligand. *Polyhedron*, 30(17): 2801-2808, 2011.

[47] Ruamps, R., Batchelor, L. J., Maurice, R., Gogoi, N., Jiménez-Lozano, P., Guihéry, N., de Graaf, C., Barra, A.-L., Sutter, J.-P. and Mallah, T. Origin of the Magnetic Anisotropy in Heptacoordinate Ni^{II} and Co^{II} Complexes. *Chemistry–A European Journal*, 19(3): 950-956, 2013.

[48] Bar, A.K., Gogoi, N., Pichon, C., Goli, V.M.L., Thlijeni, M., Duhayon, C., Suaud, N., Guihéry, N., Barra, A.L., Ramasesha, S. and Sutter, J.P. Pentagonal Bipyramid Fe^{II} Complexes: Robust Ising-Spin Units towards Heteropolynuclear Nanomagnets. *Chemistry-A European Journal*, 23(18): 4380-4396, 2017.

[49] Gogoi, N., Thlijeni, M., Duhayon, C., and Sutter, J. P. Heptacoordinated Nickel (II) as an Ising-Type Anisotropic Building Unit: Illustration with a Pentanuclear $[(NiL)_3\{W(CN)_8\}_2]$ Complex. *Inorganic Chemistry*, 52(5): 2283-2285, 2013.

[50] Liu, G.F., Filipović, M., Heinemann, F.W. and Ivanović-Burmazović, I. Seven-coordinate iron and manganese complexes with acyclic and rigid pentadentate chelates and their superoxide dismutase activity. *Inorganic Chemistry*, 46(21): 8825-8835, 2007